First Observation of Normalised Emittance Reduction through Ionization Cooling

DRAFT - MICE Internal

C. T. Rogers

Muon ionization cooling is a technique by which muon beam emittance may be reduced in order to improve the beam transmission and luminosity. Ionization cooling is a key component of proposed muon facilities such as the Muon Collider and Neutrino Factory but until now has never been demonstrated in practice.

In this paper, the effect of focussing of muons onto an energy absorber, using a very high acceptance solenoid assembly, is described. The muon phase space distribution is measured upstream and downstream of the focus. The muons are studied both with and without an energy absorber. The emittance of the muon ensemble is shown to decrease in the presence of an energy absorber and the phase space density is shown to increase, indicating that the beam has been successfully cooled.

1 Introduction

1.1 Ionisation Cooling

Ionization cooling [**?**] is the only known technique that can cool a muon beam on a timescale competitive with the muon lifetime [**?**] [**?**] [**?**] [**?**]. Muon cooling has never been demonstrated previously. In ionization cooling, a beam is passed through an absorber causing energy to be lost due to ionization of atomic electrons. This yields a reduction in normalized transverse emittance. Multiple Coulomb scattering from atoms causes an increase in angular divergence of the beam, and hence emittance growth. The change in normalized RMS emittance $\varepsilon_\perp$ in distance dz is [**?**]

$$\frac{d\varepsilon_\perp}{dz} \approx -\frac{\varepsilon_\perp}{\beta^2 E_\mu}\left\langle\frac{dE}{dz}\right\rangle + \frac{\beta_\perp(13.6\,\mathrm{MeV/c})^2}{2\beta^3 E_\mu m_\mu X_0} \tag{1}$$

where $\beta_\perp$ is the transverse optical Twiss function, βc, E_μ, m_μ are the particle velocity, energy and mass, and X_0 is the radiation length. There exists an equilibrium RMS emittance ε_{eqm}

$$\varepsilon_{eqm} \approx \frac{1}{2m_\mu}\frac{13.6^2}{X_0}\frac{\beta_\perp}{\beta\left\langle dE/dz\right\rangle} \tag{2}$$

at which $d\varepsilon_\perp/dz = 0$. If a beam with emittance below equilibrium is incident on an absorber, its emittance increases on passage through the absorber. Otherwise the emittance decreases.

1.2 The Muon Ionisation Cooling Experiment

MICE Step IV [**?**] [**?**] consists of a transfer line to bring particles from the ISIS synchrotron at Rutherford Appleton Laboratory to the cooling experiment. The cooling equipment consists of a section of a solenoid

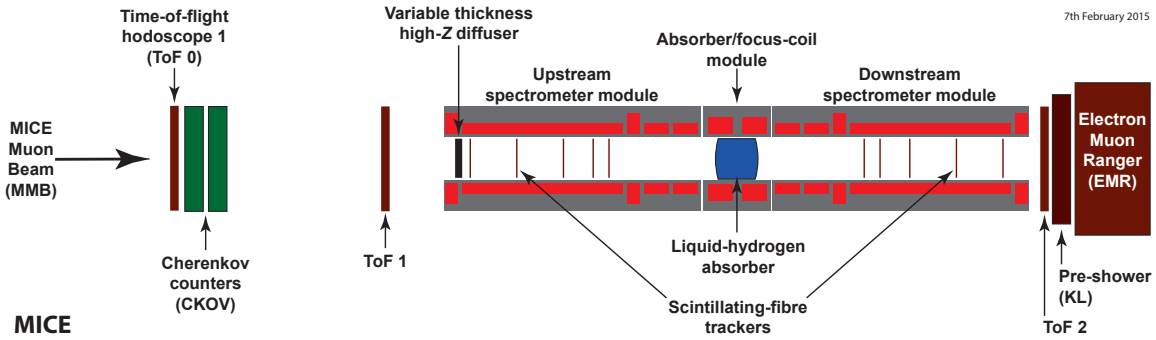

Figure 1: The MICE apparatus.

focussing ionization cooling cell. Detectors, placed upstream and downstream of the emittance reduction apparatus, measure the momentum, position and species of particles entering and leaving the cooling channel, enabling the measurement of change in normalized beam emittance of the ensemble. A schematic of the apparatus is shown in fig. 1.

1.3 Transfer Line

Pions are created by dipping a titanium target into the ISIS proton synchrotron. A dedicated transfer line has been constructed to transport the resultant particles to the cooling apparatus [**?**] [**?**] [**?**]. The incoming particle momentum can be selected by varying the field in a pair of dipoles. Higher magnetic field selects higher particle momentum. A series of tungsten and brass irises are positioned in the transfer line, enabling the selection of different emittances for the ensemble.

Up to around 100 particles are observed per second. MICE accumulates data in runs, each run consisting of a single experimental configuration and lasting of order hours. Several runs are taken for each solenoid configuration. MICE has taken data over thousands of runs, with many different configurations.

1.4 Cooling Channel

The cooling channel consists of three superconducting solenoid modules [**?**] [**?**]. Two spectrometer solenoid modules each generate a region of uniform field in which diagnostic trackers are situated and a matching region that transports the beam from the solenoid to the focus coil module. The focus coil module, positioned between the solenoids, provides additional focussing to increase the angular divergence of the beam at the absorber, improving the amount of emittance reduction that can be achieved.

The absorber was a 21 litre vessel. When filled, the absorber presents 350 mm of liquid Hydrogen along the experimental axis. Liquid hydrogen was chosen as an absorber material as it provides less multiple Coulomb scattering for a given energy loss, due to the smaller electric charge of the nucleus. Containment of the Hydrogen was provided by a pair of thin Aluminium windows. An additional pair of windows provided secondary containment in case of failure of the primary containment windows.

1.5 Diagnostic Apparatus

Upstream of the cooling apparatus, two time-of-flight detectors (TOFs) [**?**] [**?**] enable the measurement of particle velocity, which is validated by a threshold Cerenkov counter [**?**]. Scintillating fibre trackers,

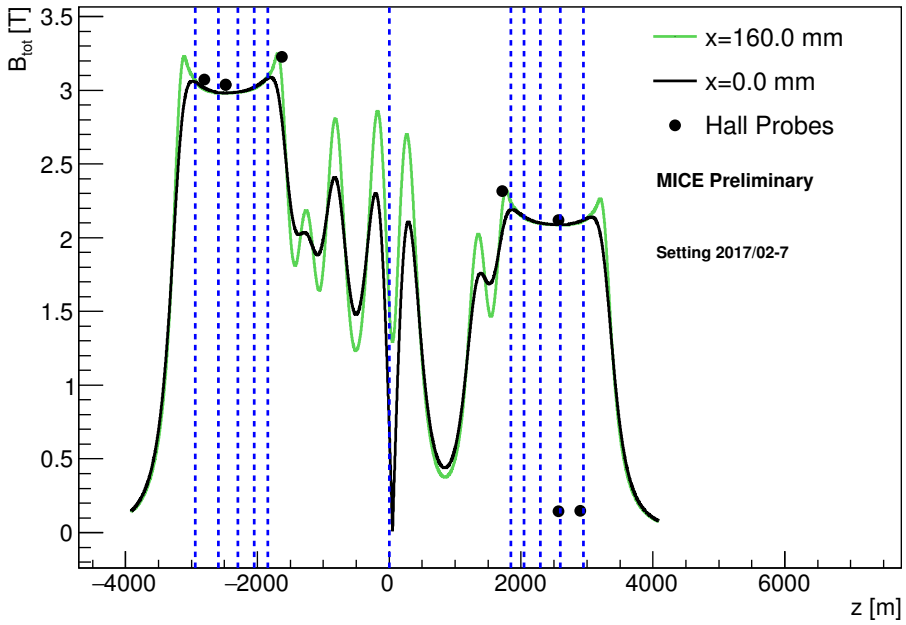

Figure 2: Modelled magnetic field for the configuration on the axis and with 160 mm horizontal displacement from the axis. Hall probes, situated 160 mm from the beam axis, show a 2 % discrepancy with the model. Dashed lines show position of the tracker stations and absorber.

positioned either side of the absorber module, enable the measurement of particle position and momentum upstream and downstream of the absorber. Further downstream an additional TOF detector, a KLOE Light pre-shower detector and Electron Muon Ranger enable rejection of electron impurities.

The trackers consist of 5 stations [**?**] [**?**]. Each station consists of 3 views, each view rotated by 120° with respect to the previous view. Each view consists of 2 layers of scintillating fibres. Gangs of 7 scintillating fibres are read out together by cryogenically operated Visible Light Photon Counters, enabling the position of incident particles to be measured with a resolution of 0.3 to 0.4 mm. The trackers are situated in uniform 3 T fields such that particles make a helical path. The magnitude of the field is measured using Hall probes situated in the region of the tracker. By measuring the radius and pitch of the helix, the momentum of the particle can be deduced. The trackers have sufficient redundancy to enable the track reconstruction to be internally validated in order to estimate the efficacy of the reconstruction. The uncertainty on the momentum of each track is around 1-2 MeV/c.

Each TOF consists of two planes. Each TOF plane is made up of a number of scintillator slabs. Photomultiplier tubes at either end of the TOF slabs produce a signal when particles pass through the TOF. The time at which muons pass through the apparatus can be measured with a resolution of 60 ps.

1.6 Operation of the Equipment

In this paper the evolution of phase space density is reported for a single configuration of the cooling magnets, '2017-02 7'. The cooling channel magnet set currents and the beam optical parameters assuming no beta-beating in the upstream spectrometer solenoid are listed in table 1. A model of the magnetic field in this configuration is shown in fig. 2.

The transfer line settings were varied to mimic different beam conditions. Results from four transfer line

Table 1: Magnet parameters and other information for 2017-02 7. The cooling channel was powered in flip mode, meaning that SSU and the upstream coil in FC had positive polarity while the downstream coil in FC and SSD had negative polarity.

Setting	2017-02 7
Full absorber runs	9946 to 9972
Full Start time	12/10/2017 11:59
Full End time	14/10/2017 12:20
Empty absorber runs	10014 to 10077
Empty Start time	18/10/2017 14:34
Empty End time	23/10/2017 09:28
Nominal FC $\beta_\perp$ [mm]	WHAT BETA FUNCTION?
Nominal momentum [MeV/c]	140
SSU Center Coil [A]	205.7
SSU Match Coil2 [A]	168.25
SSU Match Coil1 [A]	191.0
FC Coil [A]	129.24
SSD Match Coil2 [A]	195.72
SSD Center Coil [A]	144.0

configurations are reported, with the accumulated muon sample having nominal emittances of 3 mm, 4 mm, 6 mm and 10 mm at momenta around 140 MeV/c in the upstream spectrometer solenoid. These configurations are denoted '3-140', '4-140', '6-140' and '10-140' respectively.

1.7 Simulation

The cooling channel was modelled using various codes. Simulated particles based on a representative model of the pion yield from the target were transported through to the upstream edge of TOF1 using G4Beamline [**?**]. Downstream of this region, MAUS [**?**] was used to model particle transport and the response of the MICE detectors to the incoming beam.

2 Sample Selection

Update for revised cuts e.g. extrapolation cuts and global recon. List sample sizes.

2.1 Particle events

The MICE data acquisition system was set to trigger if TOF1 received simultaneous hits in a given slab. The trigger enables readout of the diagnostics during a short trigger window. All data acquired during this period is associated together and known as a particle event.

Signals in the same detector are associated into space points, for signals that are consistent with a particle passing through a given spatial region, and tracks, for signals that are consistent with a particle with a given momentum passing through a number of space points. The full reconstruction chain is described in [**?**].

2.2 Sample Selection

Particle events are selected for analysis according to a number of different criteria. Two samples are considered: the upstream sample is selected based on criteria in the upstream detector system only; the downstream sample is selected from the upstream sample, based on additional criteria in the downstream detector system. Because the upstream sample is selected based on measurements in the upstream detector system, the upstream sample is independent of any stochastic processes occurring in the absorber.

The sample selection criteria are detailed in Table **??** together with the number of events surviving each cut. The criteria are described in detail below.

Table 2: The sample selection criteria are listed sequentially, in the order that the selection was made. The number of events surviving the selection and all preceding selections is listed for each of the data runs studied in this note.

cut	2017-2.7 3-140 None	2017-2.7 3-140 lH2 empty	2017-2.7 3-140 lH2 full	2017-2.7 3-140 LiH	2017-2.7 6-140 None	2017-2.7 6-140 lH2 empty	2017-2.7 6-140 lH2 full	2017-2.7 6-140 LiH	2017-2.7 10-140 None	2017-2.7 10-140 lH2 empty	2017-2.7 10-140 lH2 full	2017-2.7 10-140 LiH
all events	258683	172444	183035	240396	258972	177328	283405	307300	391666	209994	374910	471965
tof 1 sp	249235	166313	177064	231587	250774	171124	275269	296958	370498	196606	356829	441852
tof 0 sp	196955	133090	146186	183288	198333	132548	226008	229741	283105	144999	281242	326715
scifi tracks us	74993	51170	56756	70331	135115	91156	152464	158491	150299	77015	148135	174896
scifi nan us	74993	51170	56756	70331	135115	91156	152464	158491	150299	77015	148135	174896
chi2 us	74993	51170	56756	70331	135115	91156	152464	158491	150299	77015	148135	174896
scifi fiducial us	74845	51083	56614	70188	134952	91058	152294	158341	149056	76395	146885	173477
delta tof01	42256	28799	32738	41667	65251	44170	83405	84264	74228	38726	87960	99222
tof01	38706	26179	28150	36889	56501	37444	63544	66922	56341	28995	61434	68642
p tot us	14291	9372	9836	12956	21985	14575	24002	25181	14541	7507	15353	17275
global through tof0	14283	9365	9817	12945	21924	14508	23799	25001	13779	6957	13177	15170
upstream aperture cut	13789	9158	9605	12536	21532	14283	23398	24589	10779	5418	10607	12188
upstream cut	13789	9158	9605	12536	21532	14283	23398	24589	10779	5418	10607	12188
scifi tracks ds	13615	8986	9315	12293	20929	13795	22504	23798	10220	5051	9787	11296
scifi nan ds	13615	8986	9315	12293	20929	13795	22504	23798	10220	5051	9787	11296
chi2 ds	13615	8986	9315	12293	20929	13795	22504	23798	10220	5051	9787	11296
scifi fiducial ds	13615	8986	9315	12293	20929	13795	22504	23798	10220	5051	9787	11296
p tot ds	13365	8845	9169	12093	20634	13589	22163	23482	10093	4994	9655	11188
downstream cut	13365	8845	9169	12093	20634	13589	22163	23482	10093	4994	9655	11188
downstream aperture cut	7423	4824	5246	6945	12487	8307	13398	14299	4637	2347	4319	5080
tof 2 sp	7145	4598	4959	6583	11900	7851	12576	13412	4412	2212	3979	4675
global through tkd tp	7145	4598	4959	6583	11900	7851	12576	13412	4412	2212	3979	4675
global through tof2	7145	4598	4959	6583	11900	7851	12576	13412	4412	2212	3979	4675
extrapolation cut	7145	4598	4959	6583	11900	7851	12576	13412	4412	2212	3979	4675

Table 3: Simulated sample selection

cut	Simulated 2017-2.7 3-140 None	Simulated 2017-2.7 3-140 lH2 empty	Simulated 2017-2.7 3-140 lH2 full	Simulated 2017-2.7 3-140 LiH	Simulated 2017-2.7 6-140 None	Simulated 2017-2.7 6-140 lH2 empty	Simulated 2017-2.7 6-140 lH2 full	Simulated 2017-2.7 6-140 LiH	Simulated 2017-2.7 10-140 None	Simulated 2017-2.7 10-140 lH2 empty	Simulated 2017-2.7 10-140 lH2 full	S 2
all events	160522	160748	159335	159273	222654	220316	220412	220685	302493	303203	298029	
tof 1 sp	150492	150532	149144	149068	211790	210051	209874	210365	289108	289886	284938	
tof 0 sp	146435	146304	145015	144826	206009	204310	203969	204661	282471	283220	278573	
scifi tracks us	62520	62198	62119	62083	138715	136949	140464	140862	143767	143858	141413	
scifi nan us	62520	62198	62119	62083	138715	136949	140464	140862	143767	143858	141413	
chi2 us	62520	62198	62119	62083	138715	136949	140464	140862	143767	143858	141413	
scifi fiducial us	61897	61579	61508	61456	138202	136470	139952	140375	141368	141596	139171	
delta tof01	35124	35505	39444	38673	58627	59508	70744	69823	75446	77905	90060	
tof01	32112	32289	32661	32262	43543	42274	45133	44787	55239	56400	59685	
p tot us	9701	9670	9880	9838	13775	14531	13808	13819	11424	11727	12277	
global through tof0	9581	9412	9435	9551	13603	14301	13431	13455	10051	9823	8596	
upstream aperture cut	8791	8822	8899	8905	13245	13998	13144	13160	6406	6217	6312	
upstream cut	8791	8822	8899	8905	13245	13998	13144	13160	6406	6217	6312	
scifi tracks ds	8689	8695	8728	8777	12708	13391	12572	12669	6008	5834	5833	
scifi nan ds	8689	8695	8728	8777	12708	13391	12572	12669	6008	5834	5833	
chi2 ds	8689	8695	8728	8777	12708	13391	12572	12669	6008	5834	5833	
scifi fiducial ds	8689	8695	8728	8777	12708	13391	12572	12669	6008	5834	5833	
p tot ds	8579	8551	8532	8662	12529	13148	12331	12533	5949	5740	5692	
downstream cut	8579	8551	8532	8662	12529	13148	12331	12533	5949	5740	5692	
downstream aperture cut	5078	5053	5160	5162	7450	7834	7179	7146	2729	2622	2466	
tof 2 sp	4671	4640	4697	4662	6742	7079	6428	6335	2443	2386	2191	
global through tkd tp	4671	4640	4697	4662	6742	7079	6428	6335	2443	2386	2191	
global through tof2	4671	4640	4697	4662	6742	7079	6428	6335	2443	2386	2191	
extrapolation cut	4671	4640	4697	4662	6742	7079	6428	6335	2443	2386	2191	
upstream cut	8791	8822	8899	8905	13245	13998	13144	13160	6406	6217	6312	
mc muon us	8790	8821	8897	8904	13242	13996	13140	13157	6405	6217	6311	
mc stations us	8790	8821	8897	8904	13242	13996	13140	13157	6405	6217	6311	
mc scifi fiducial us	8790	8821	8897	8904	13242	13996	13140	13157	6405	6217	6311	
mc true us cut	8790	8821	8897	8904	13242	13996	13140	13157	6405	6217	6311	

Table 4: Upper and lower bound of TOF cuts for different beamline settings.

Beamline	Lower Bound [ns]	Upper Bound [ns]
3-140	27.0	32.0
6-140	27.0	31.0
10-140	27.0	30.0

2.3 Upstream Sample

Cuts applied to the upstream sample are described below.

KL: Add aperture cuts for downstream apertures

- One TOF1 Space Point: Events have exactly one space point reconstructed in TOF1.
- One TOF0 Space Point: Events have exactly one space point reconstructed in TOF0.
- One TKU Track: Events have exactly one track reconstructed in TKU, with finite position and momentum and associated error matrices.
- TKU χ^2 per degree of freedom: The reconstructed χ^2 per degree of freedom in TKU is required to be less than 10. The χ^2 per degree of freedom of events in each sample is shown in fig. **??**.
- TKU fiducial cut: Events are required to have a maximum radial excursion in TKU less than 150 mm. The maximum radial excursion of the track is estimated assuming a helical trajectory between tracker stations. The maximum radial excursion of events in each sample is shown in fig. **??**.
- TKU Momentum: Events are required to have momentum reconstructed by TKU between 135 and 145 MeV/c. The momentum of events in each sample is shown in fig. **??**.
- TOF01 Time: Pions and electrons in the momentum selection described above have a quite different time-of-flight between TOF0 and TOF1 to muons. Events are required to have time-of-flight between TOF0 and TOF1 consistent with a muon in order to reject this background. The time-of-flight of events in each sample is shown in fig. **??**. The velocity of particles upstream of the diffuser is faster for thicker diffuser settings, in order to yield a muon sample with momentum peaked around 140 MeV/c in TKU. In order to correctly reject impurities, the TOF01 cut is different for different beamline settings, as listed in table 4
- Delta TOF01 Time: DESCRIPTION

Events which do not meet these criteria are not considered for analysis at all.

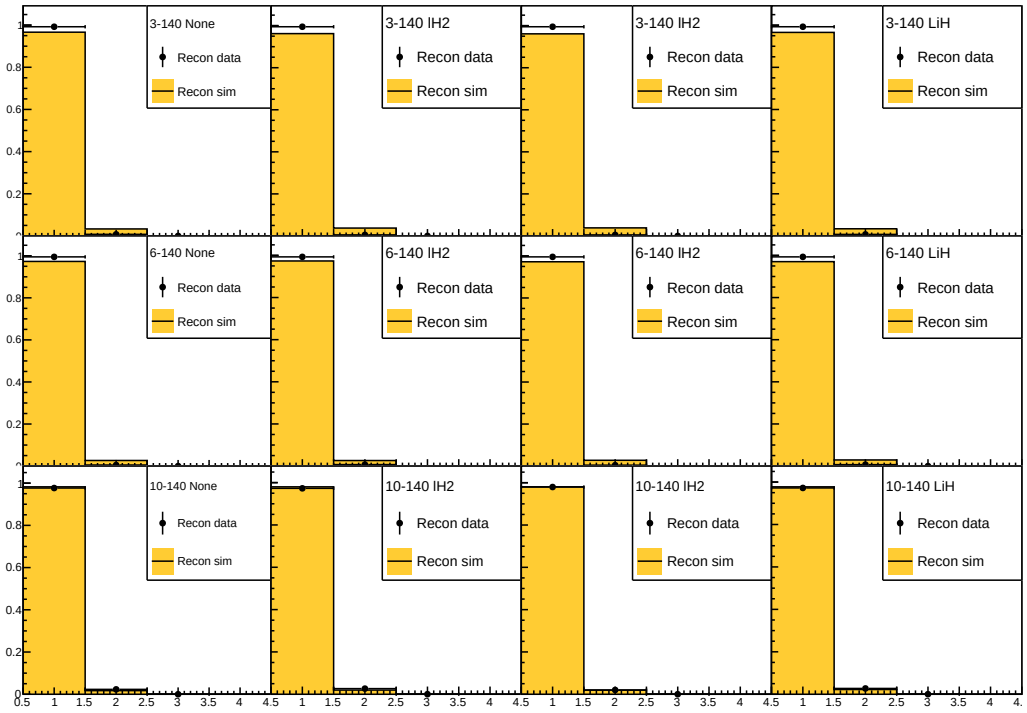

Number of space points in TOF1

Figure 3: Number TOF1 space points.

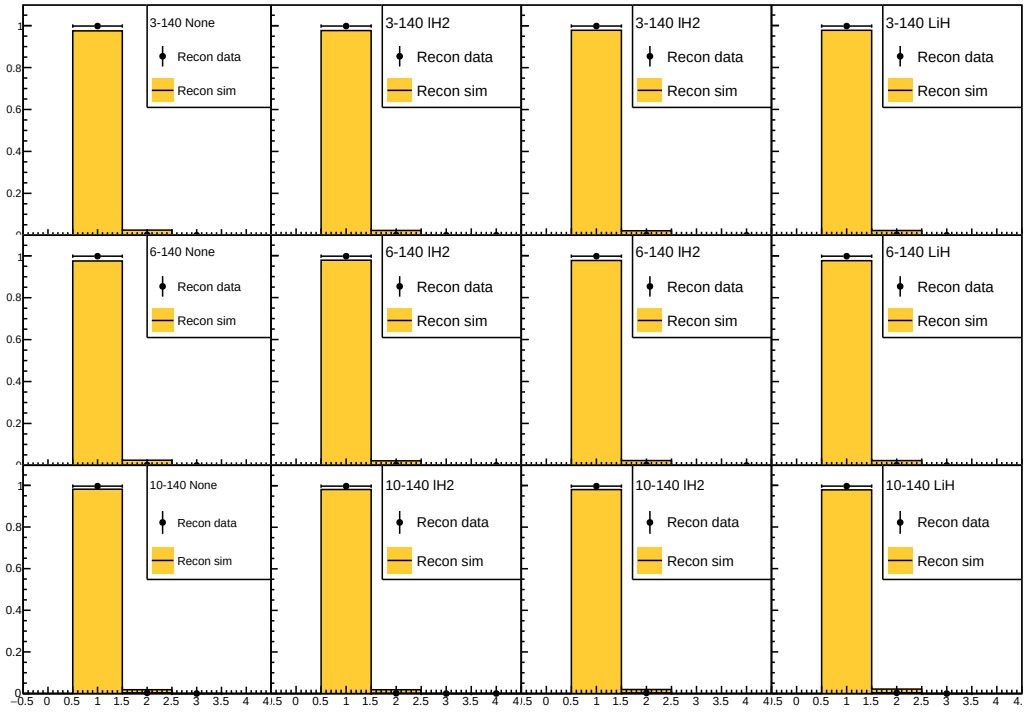

Number of space points in TOF0

Figure 4: Number TOF0 space points.

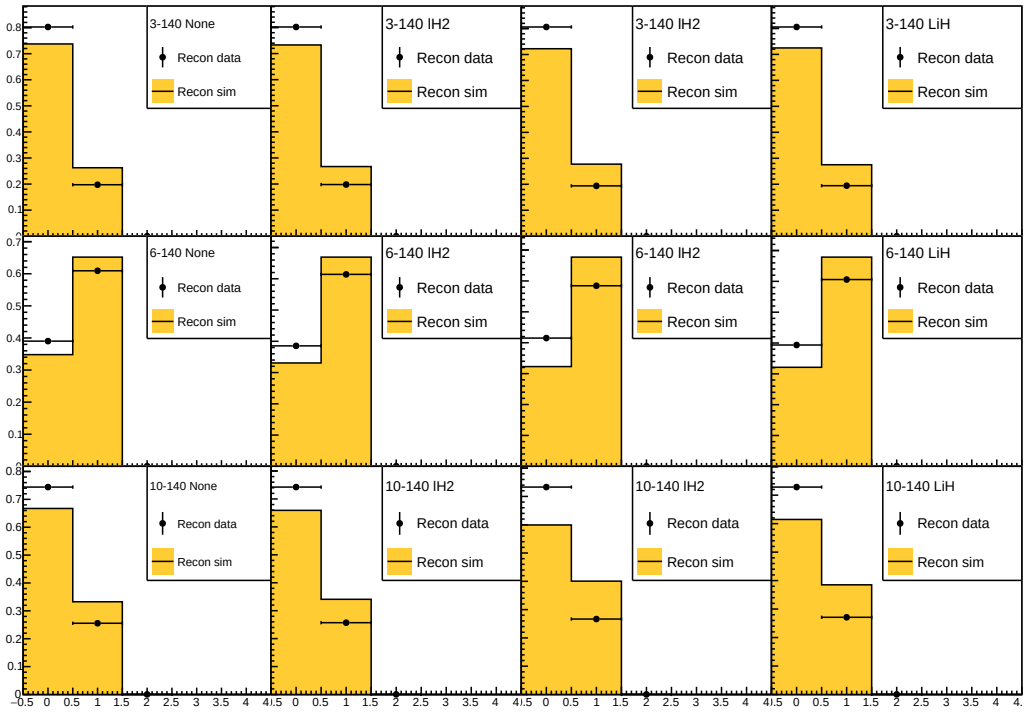

Figure 5: N tracks.

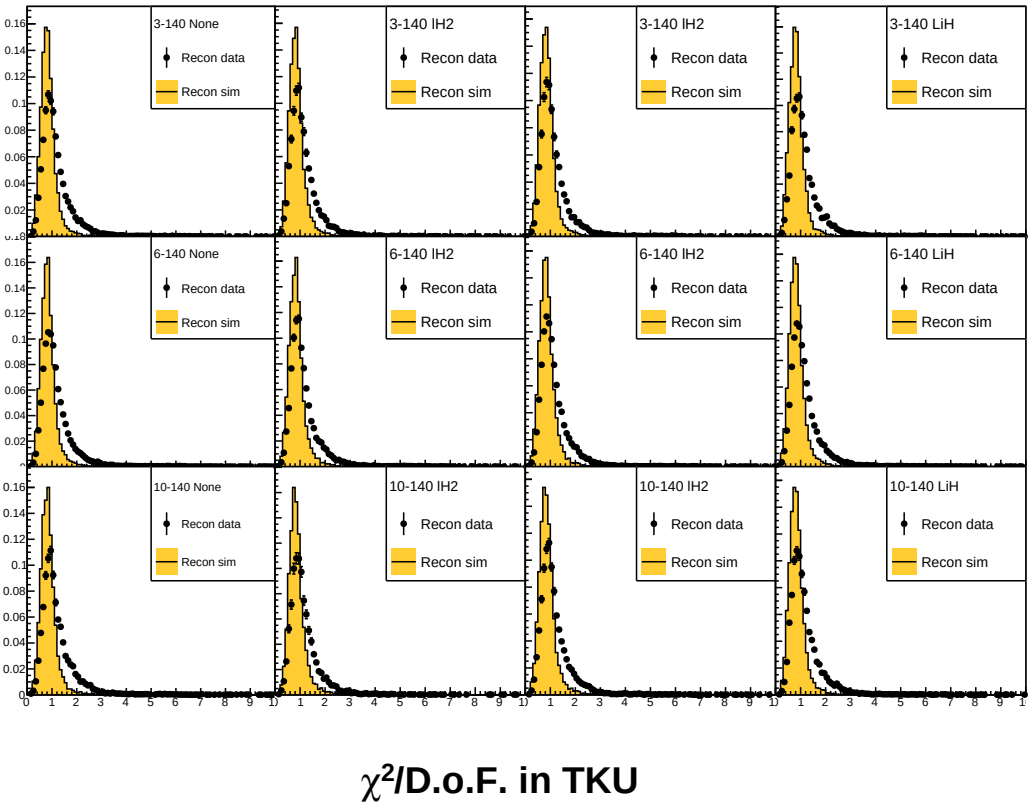

Figure 6: χ^2 per degree of freedom distribution in TKU for 3-140 beam (top), 6-140 beam (middle) and 10-140 beam (bottom). The left hand column shows data with full absorber; the right hand column shows data with empty absorber. The black line shows all events; red shows events in the upstream sample; green shows events in the downstream sample.

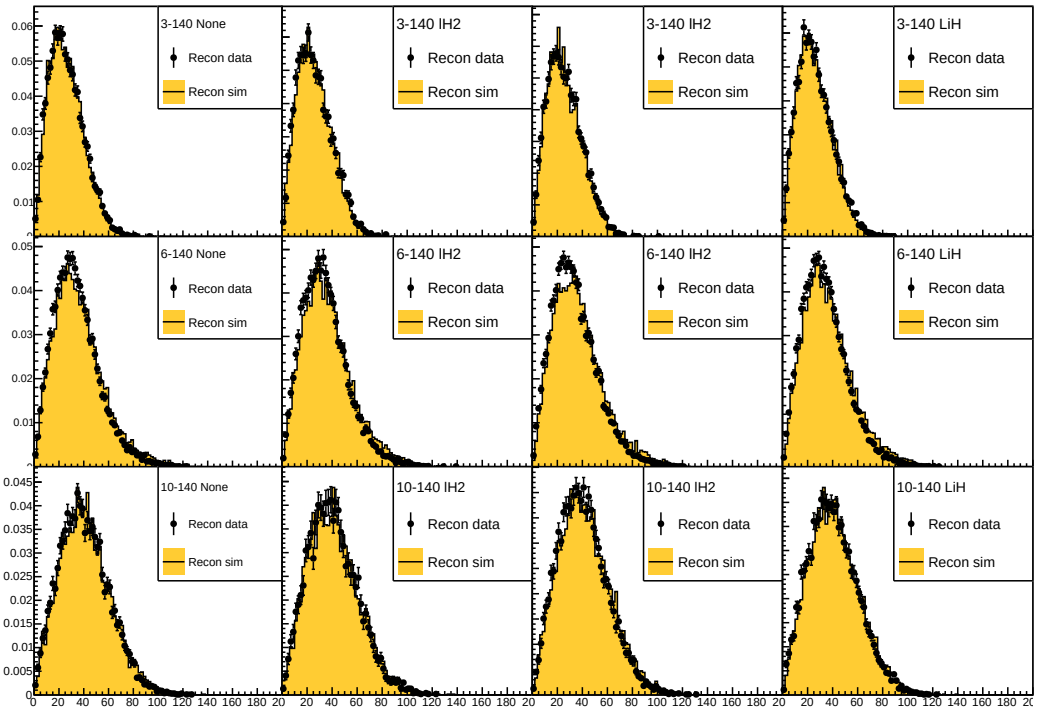

Figure 7: Maximum radius.

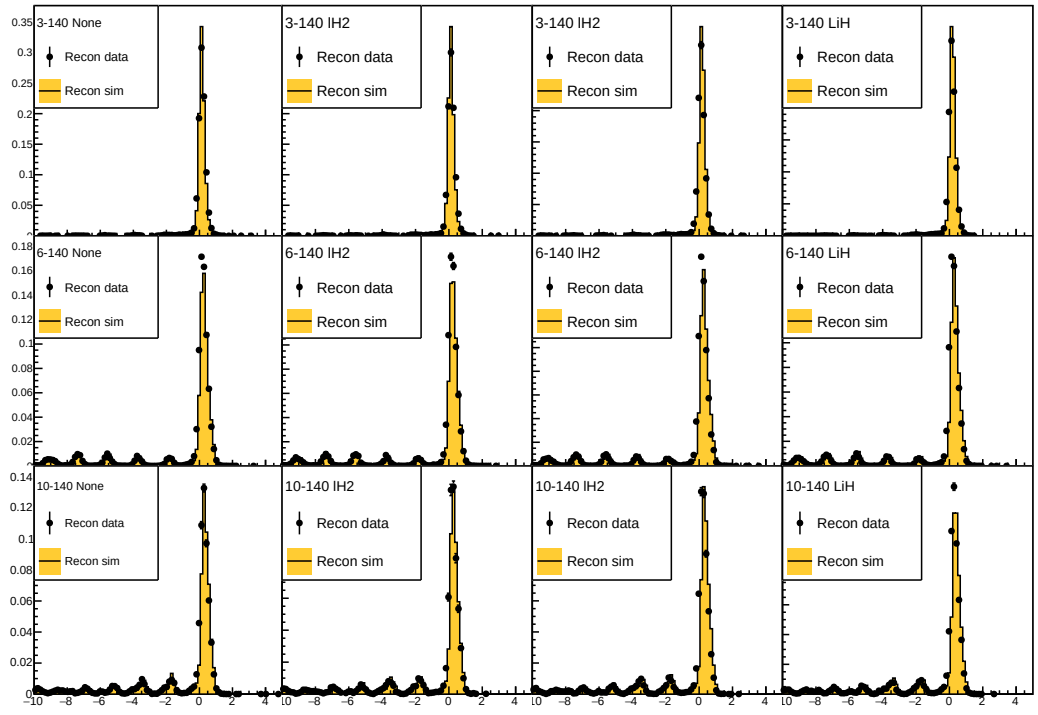

Figure 8: delta tof01.

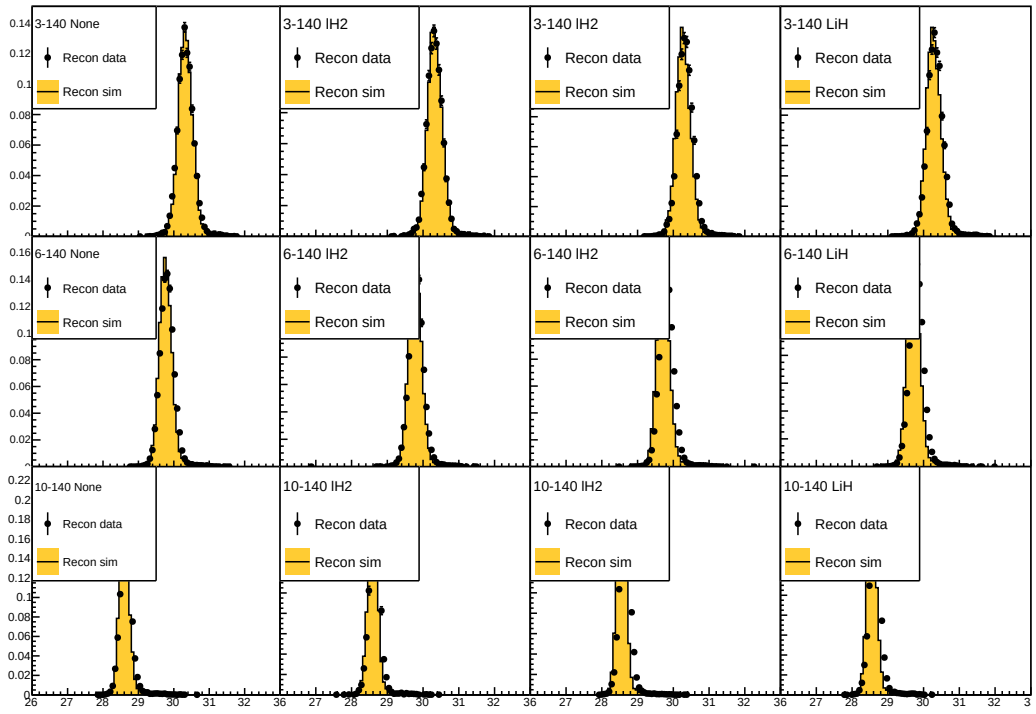

Figure 9: Time-of-flight measured between TOF0 and TOF1 for 3-140 beam (top), 6-140 beam (middle) and 10-140 beam (bottom). The left hand column shows data with full absorber; the right hand column shows data with empty absorber. The black line shows all events; red shows events in the upstream sample; green shows events in the downstream sample.

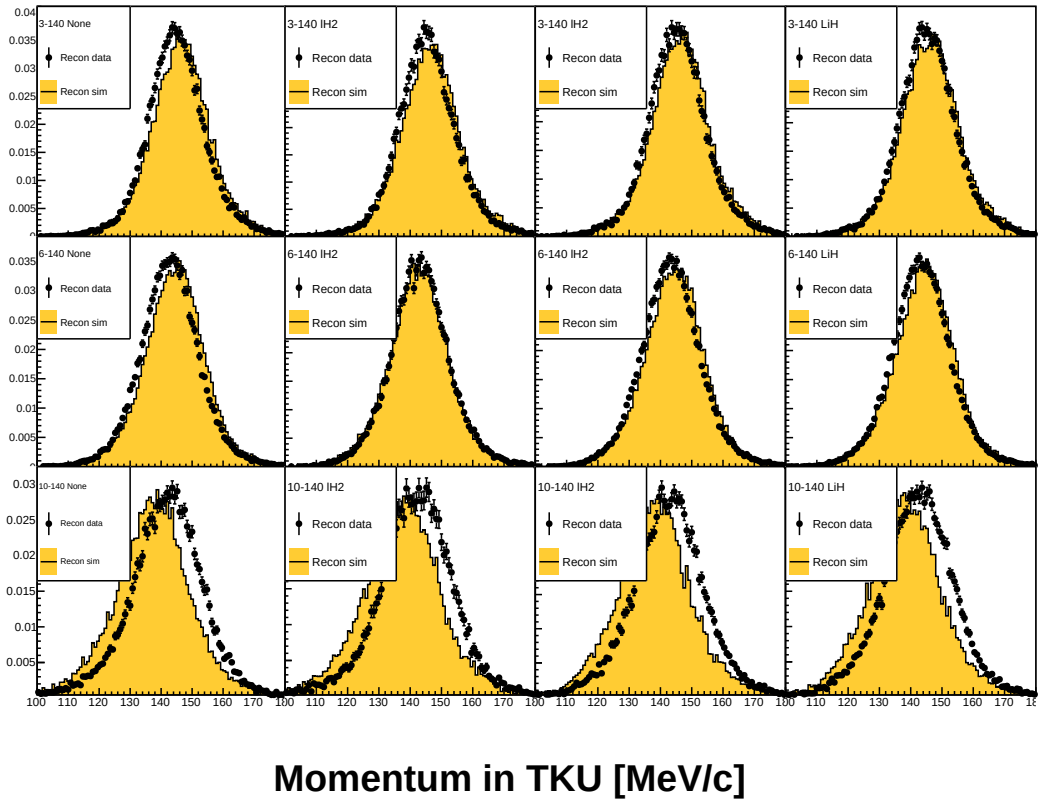

Figure 10: Momentum measured by TKU for 3-140 beam (top), 6-140 beam (middle) and 10-140 beam (bottom). The left hand column shows data with full absorber; the right hand column shows data with empty absorber. The black line shows all events; red shows events in the upstream sample; green shows events in the downstream sample.

2.4 Downstream Sample

Cuts applied to the downstream sample are described below.

- In Upstream Sample: Events are required to be in the upstream sample to be considered in the downstream sample.
- One TKD Track: Events have exactly one track reconstructed in TKD.
- TKD Momentum: Events are required to have reconstructed momentum between 100 and 200 MeV/c. The momentum as reconstructed by TKD of events in each sample is shown in fig. **??**
- TKD χ^2 per degree of freedom: The reconstructed χ^2 per degree of freedom in TKD is required to be less than 10. The χ^2 per degree of freedom of events in each sample in TKD is shown in fig. **??**.

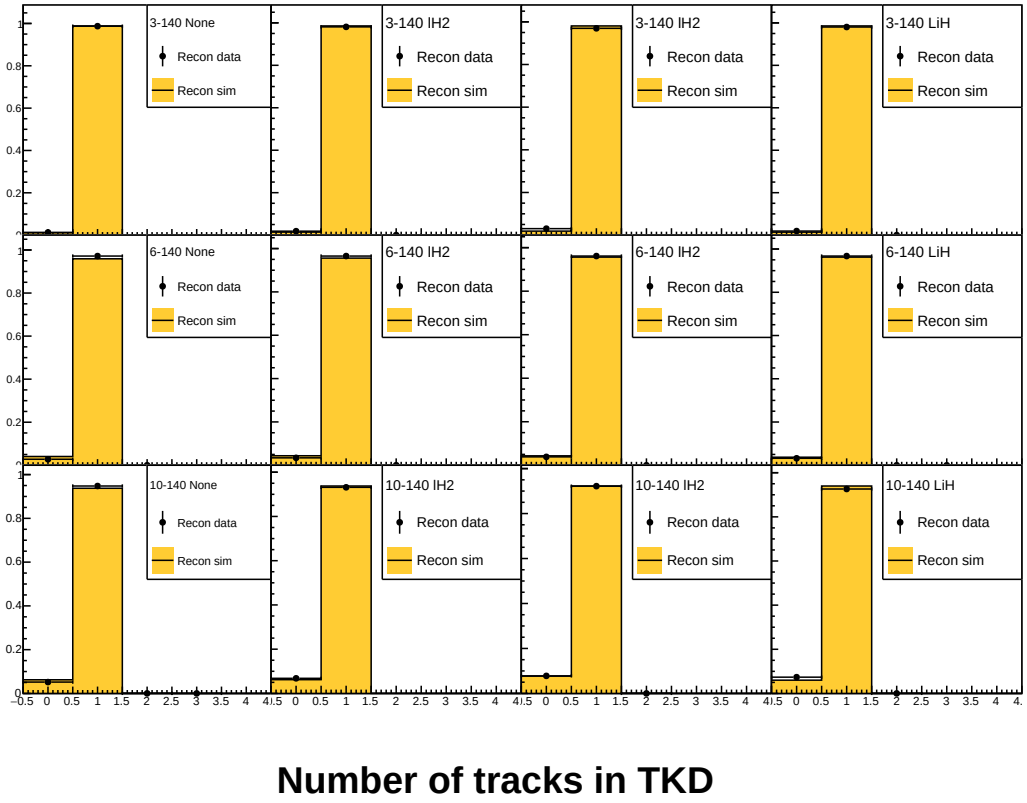

Figure 11: The number of tracks measured in TKD, with the requirement that the number of tracks is 1 disabled.CHECK - is this really right? Where are events with no tracks recorded

Events which do not meet these downstream sample criteria are not considered for analysis in the downstream region. They may either have collided with the cooling channel aperture and been lost (scraping), or they may have been not observed by the detectors (inefficiency). Systematic correction and uncertainty due to detector inefficiency is discussed in Section **??**.

3 Detectors

In this section, the resolution and efficiency of the detector systems is discussed. The reconstruction is validated both internally within each detector system, using the detector's internal redundancy, and by extrapolating reconstructed events between detectors.

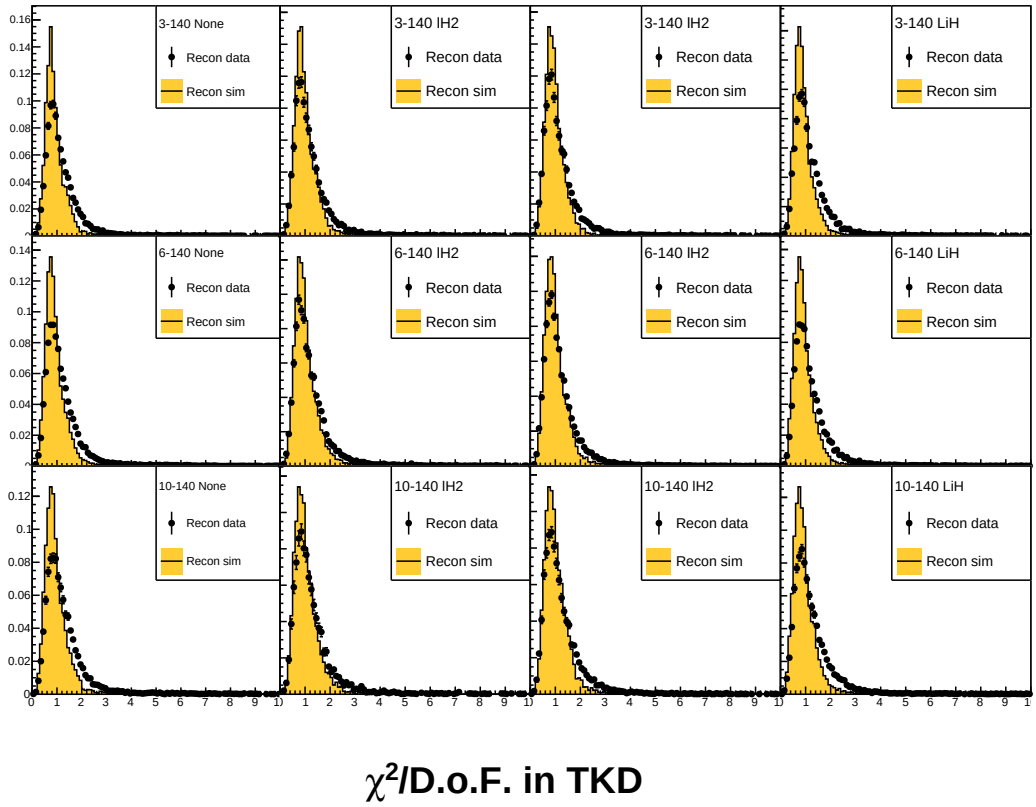

Figure 12: χ^2 distribution in TKD for all events in the downstream sample, with the maximum radius cut disabled.

3.1 Tracker

References

Two trackers, made up of five stations each with three planes of scintillating fibres are used to reconstruct the momentum of incoming particles. Particles make helical trajectories whose radius and wavelength vary according to the transverse and longitudinal momentum respectively. The radius of the helix is given approximately by

$$r = \frac{p_t}{qB_z} \tag{3}$$

and the wavenumber by

$$k = \frac{qB_z}{p_z}. \tag{4}$$

Fitting is performed in several steps. Electronics signals arising from adjacent fibres are collected into clusters. The position of clusters in adjacent planes are collected to form a space point. A first-pass fit of a perfect helix to the space points, pattern recognition, is used for noise rejection and to seed a second-pass fit using a Kalman filter.

4 Resolution

If the reconstruction is well-understood, the path of the reconstructed trajectories should match the position of the clusters. The χ^2 distribution per degree of freedom of reconstructed tracks was shown in fig. **??** and **??** for the upstream and downstream detectors respectively.

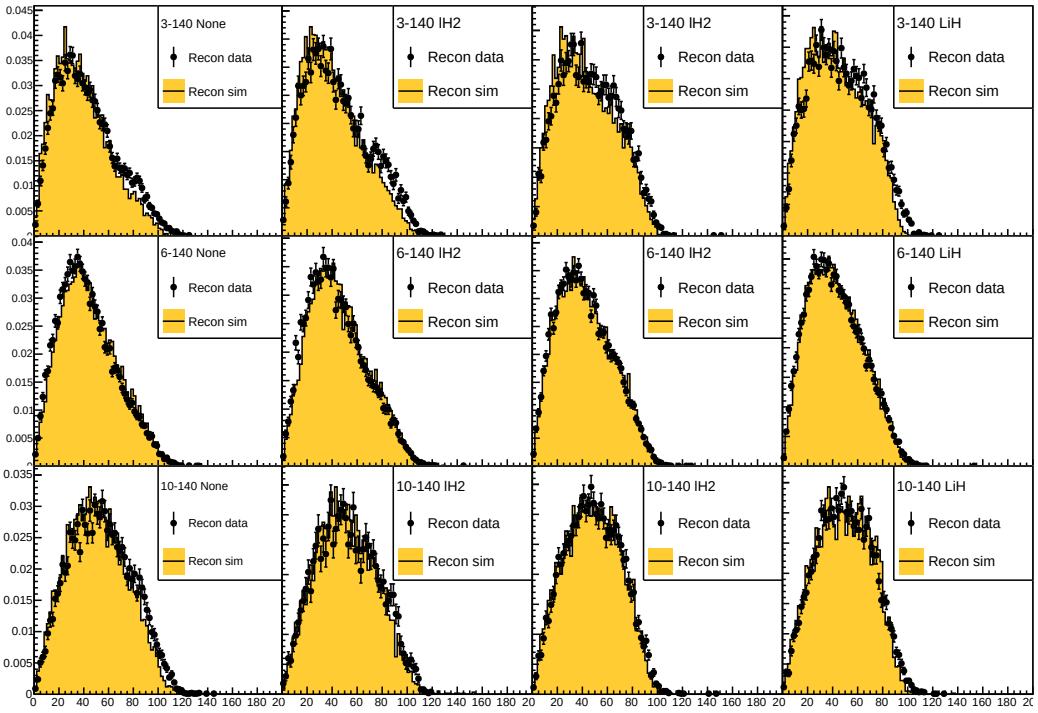

Figure 13: Maximum radius in TKD at each tracker station for all events in the downstream sample, with the maximum radius cut disabled.TODO - calculate the track radius between stations, as well as at each station

In order to accurately reconstruct tracks the field must be well known. If the modelled field used in reconstruction differs from the actual field, a helix can be found but the reconstructed longitudinal and transverse momenta will scale with the field according to eq. (3) and eq. (4). In order to accurately reconstruct the field correctly it is essential to understand the field accurately in the measurement region.

The field in the tracker region was monitored during the data taking period by several Hall probes. The Hall probe measurement in the tracker region is shown in fig. 15 for the data taking periods under study in this paper. Reproducibility is demonstrated at around the 10^{-3} T level for HP67 and around 10^{-4} T level for the other hall probes.

The measured fields are shown overlayed with the modelled field in the tracker region in fig. 16. There is some disagreement between the model and the hall probe readings, particularly in the fringe field of the magnets.

An additional level of validation is provided by extrapolating the measured particle trajectories between detector systems. This is discussed below.

5 Inefficiency and Impurity

The efficiency of track-finding can be studied. This analysis will count the change in the number of events in different bins in amplitude. Impurity can lead to an overestimation of the number of events in a bin. Inefficiency can lead to an underestimation of the number of events in a bin. Because the sample is defined according to events measured in the upstream tracker, only inefficiency in the downstream tracker contributes to uncertainties in this analysis. Impurity in both trackers can contribute to uncertainties.

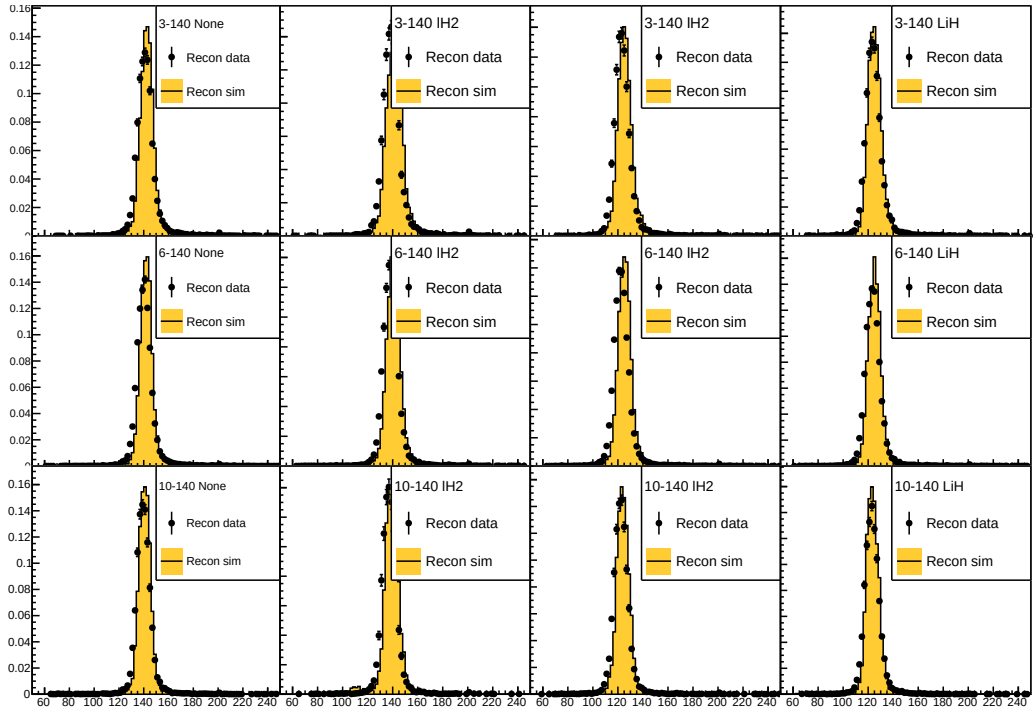

Figure 14: Momentum in TKD, for all events in the downstream sample with the the total momentum cut disabled.

The inefficiency can be estimated by studying the response in detectors other than the tracker and comparing this with the tracker response. The number of clusters in events contained within the upstream sample, not making a TKD track but making exactly one TOF2 space point is shown in fig. **??**. These tracks are candidates for reconstruction inefficiency; they may be real particles that did not make a track, for example due to excess scattering leading to a rejection by the pattern recognition phase of the reconstruction.

Impurity can arise due to noise in the tracker readout, leading to clusters and even tracks that are not associated with a particle. The magnitude can be estimated in TKU by studying the number of planes that register at least one cluster in events that pass the TOF01 cuts but did not make a TKU track. By observing the amount of noise in the tracker, one can infer the number of impure tracks. The distribution of noise for these events is shown in fig. **??**. There is a clear separation between the peak corresponding to noise tracks and the peak corresponding to real tracks for all but the highest emittance beams. Quantitative estimates will be made in section on errors.

Add distribution in chi2 from Pattern Recognition?

The magnitude can be estimated similarly in TKD by studying the number of clusters in events that pass the upstream cuts but did not make a TKD track or a TOF2 space point. These events are expected to correspond to events where no particle traversed the detector. This is shown in **??**. There is a clear separation between the peak corresponding to noise tracks and the peak corresponding to real tracks for all but the highest emittance beams. Quantitative estimates will be made in section on errors.

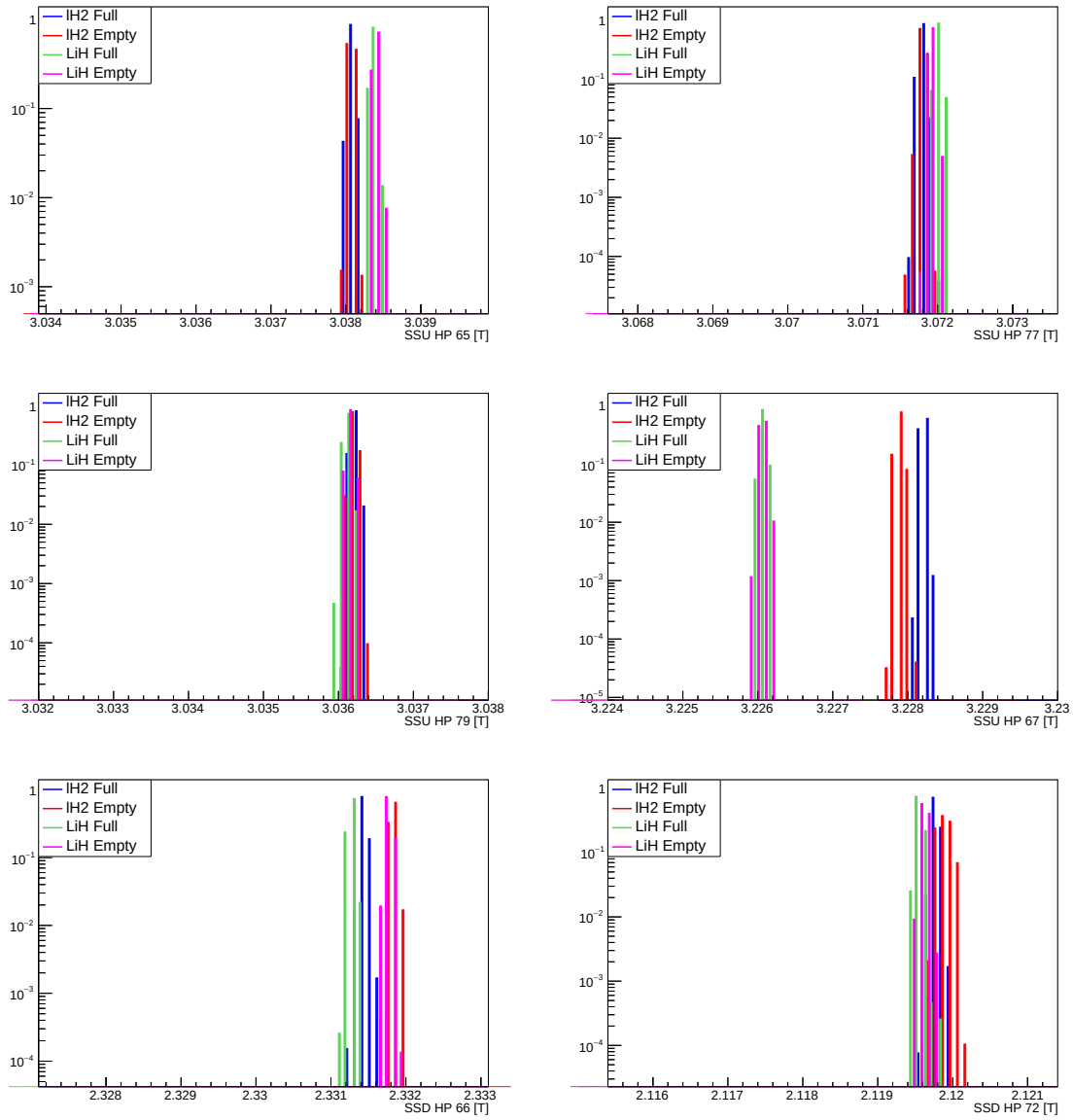

Figure 15: Hall probe readings for the four datasets across the entire period where data was taken.

5.1 TOF

Three TOF stations are used to measure the time at which particles pass through the experiment. The TOF stations consist of two layers aligned at right angles, each made up of several scintillating plastic slabs. Each slab has a PMT at either end that records the time at which particles pass through the detector. Reconstruction software searches for coincidences of the PMTs at either end of a slab and coincidences of slabs in each layer in order to make a TOF ”space point”. A calibration is applied to account for cable lengths and correct for so-called “time walk” that arises due to a different PMT response for a different charge deposited by the PMT.

The TOF resolutions can be estimated by comparing the reconstructed time between each slab, after calibration. This is shown for each of the TOF detectors in fig. **??**, **??** and **??**. As the TOF is only used for validation of the tracker and for PID in the upstream region, impurity and inefficiency in the TOF does not affect this analysis.

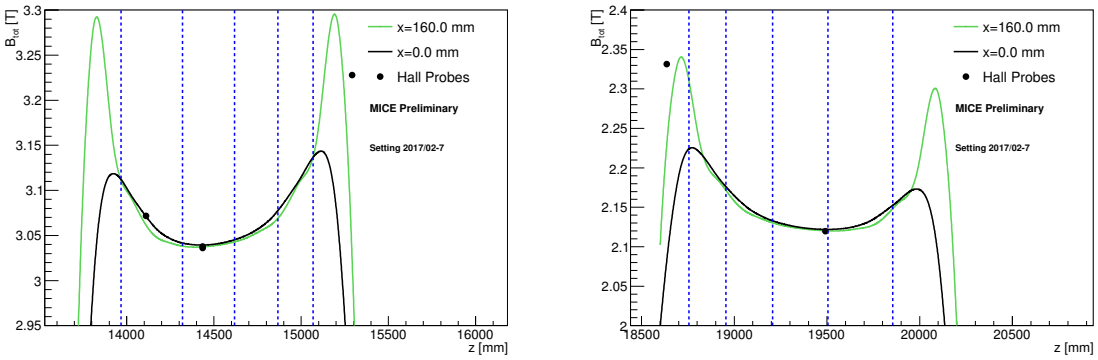

Figure 16: Hall probe readings compared to the field model used for reconstruction and track extrapolation. Blue dashed lines show the position of the tracker stations.

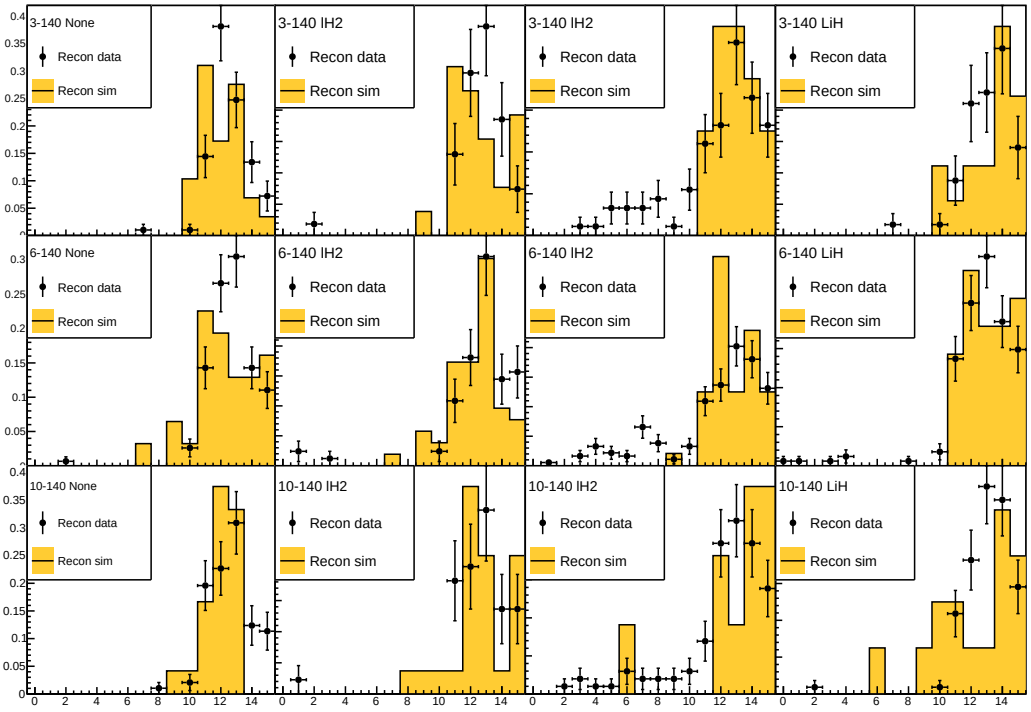

Figure 17: Number of planes in TKD that contain at least one cluster. Here we take all events in the upstream sample, and add the requirement that exactly one space point was reconstructed in TOF2 and no track was reconstructed in TKD. The events with more than about 10 clusters are suspected of having a real particle in TKD that was not reconstructed by the pattern recognition routines; while the events with fewer than 10 clusters are suspected of having a noise event in TOF2.

6 Global reconstruction

The overall detector performance can be validated by extrapolating tracks from one detector to another and comparing the reconstructed coordinates with the extrapolated values. Tracks measured in the upstream tracker are extrapolated upstream to TOF1 and TOF0, and downstream to TKD and TOF2. Where there are materials

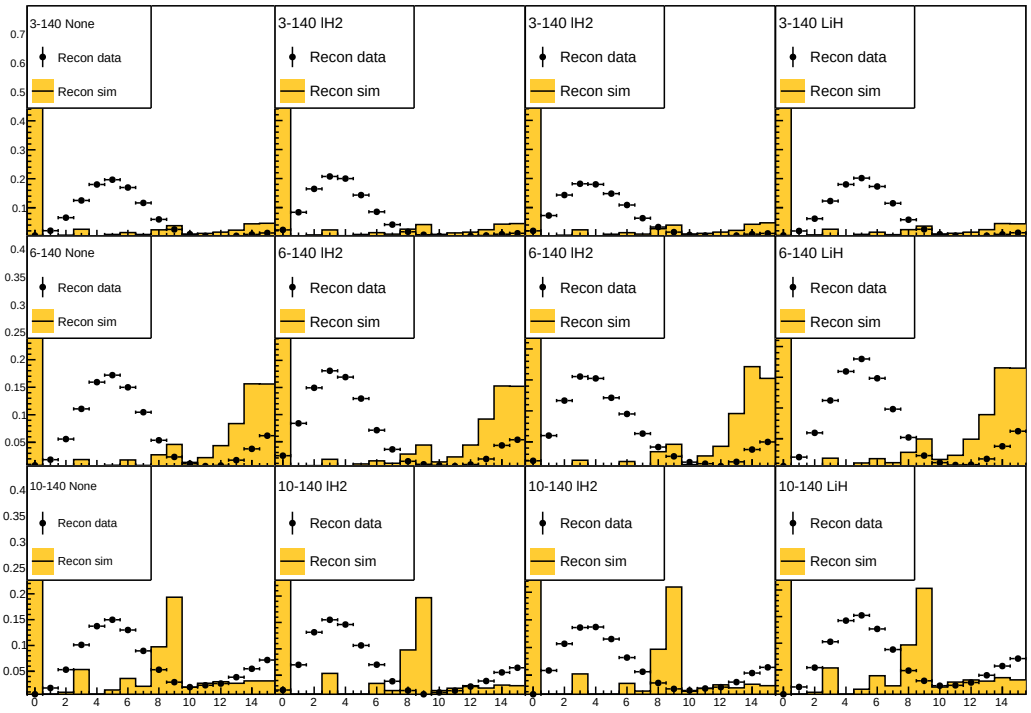

Figure 18: Number of planes in TKU that contain at least one cluster. Here we take all events in the upstream sample, except we require that no TKU track was constructed. The peak at 15 planes are real particles in TKU that were not reconstructed. The peak at 5 planes arises due to noise. In the overlap region, a few events may have sufficient clusters to produce a track, which could lead to impurity.

in the beamline, the energy change on passing through the material is estimated using the most probably energy loss, as given by [**?**] DO EQUATION

$$anequation \tag{5}$$

Material thicknesses are approximated by the on-axis thickness. In order to reduce the effect of scattering from apertures, only events whose projected trajectory is significantly distant from the apertures are considered in this analysis.

The extrapolated position following extrapolation to TOF1 is shown in fig. **??** and **??**. Intepretation??

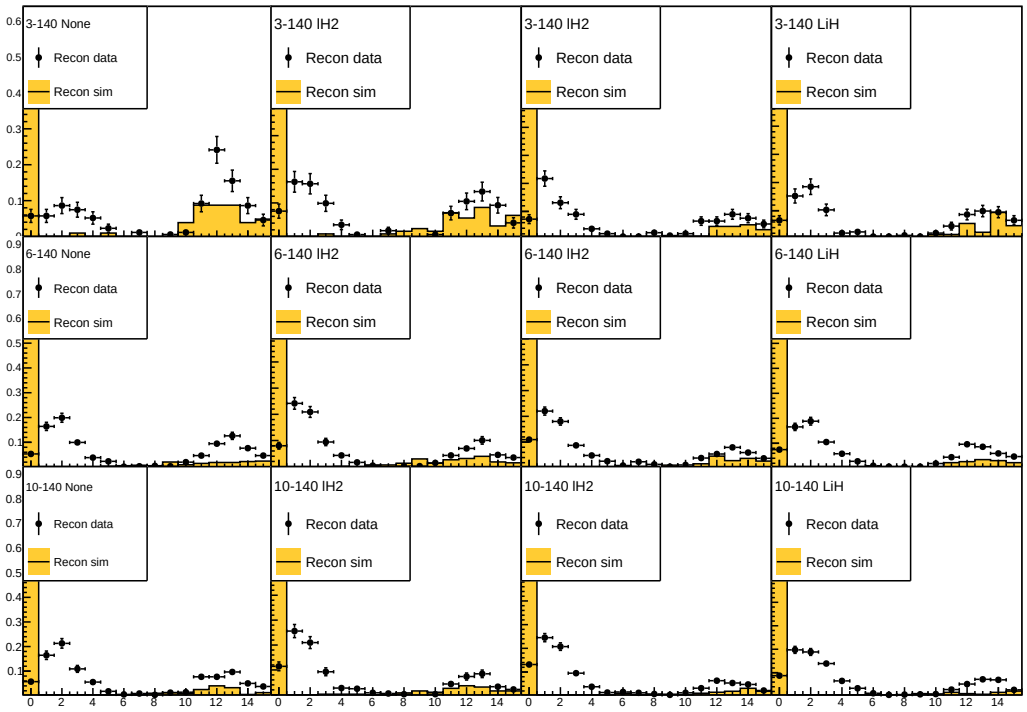

Figure 19: Number of planes in TKD that contain at least one cluster. Here we take all events in the upstream sample, and add the requirement that no track was reconstructed in TKD. The peak at 15 planes are real particles in TKD that were not reconstructed. The peak at 5 planes arises due to noise. In the overlap region, a few events may have sufficient clusters to produce a track, which could lead to impurity due to noise.

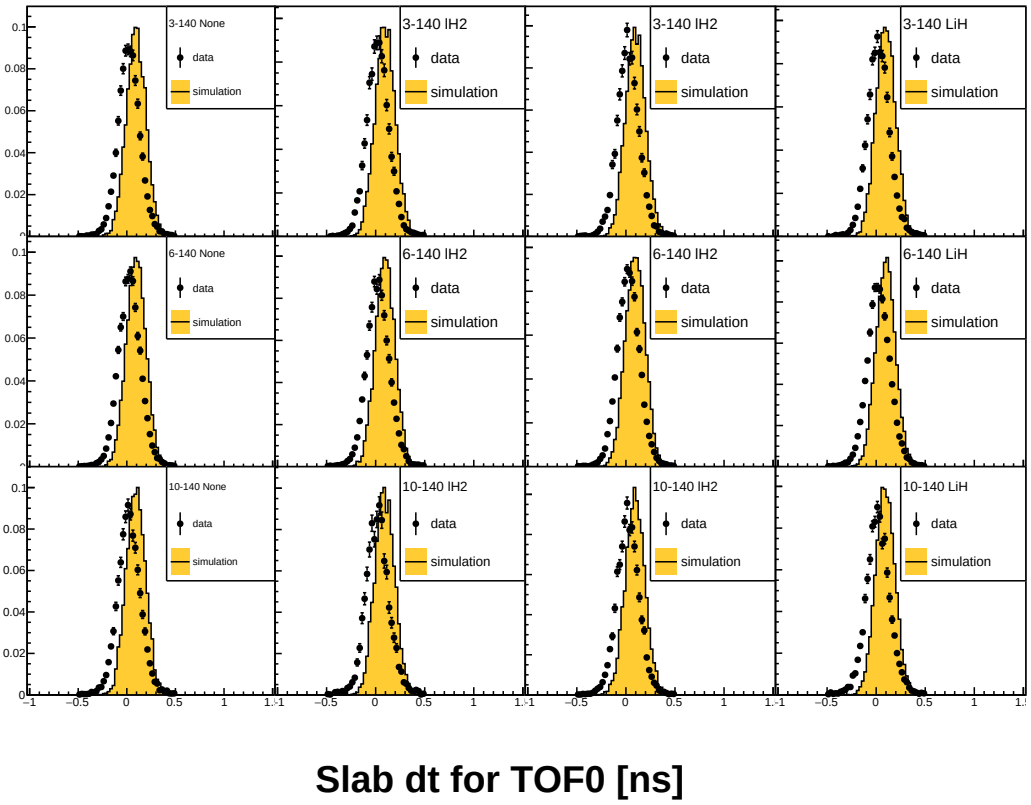

Figure 20: Measured time difference between adjacent TOF0 slabs for events in the upstream sample.

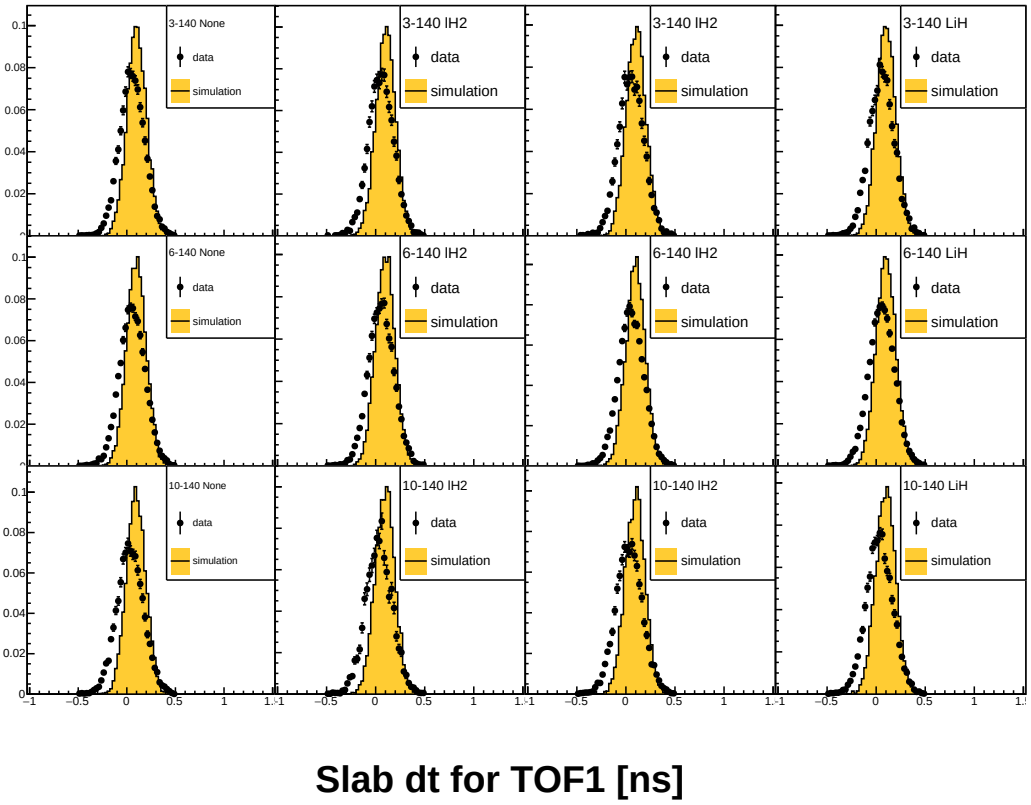

Figure 21: Measured time difference between adjacent TOF1 slabs for events in the upstream sample.

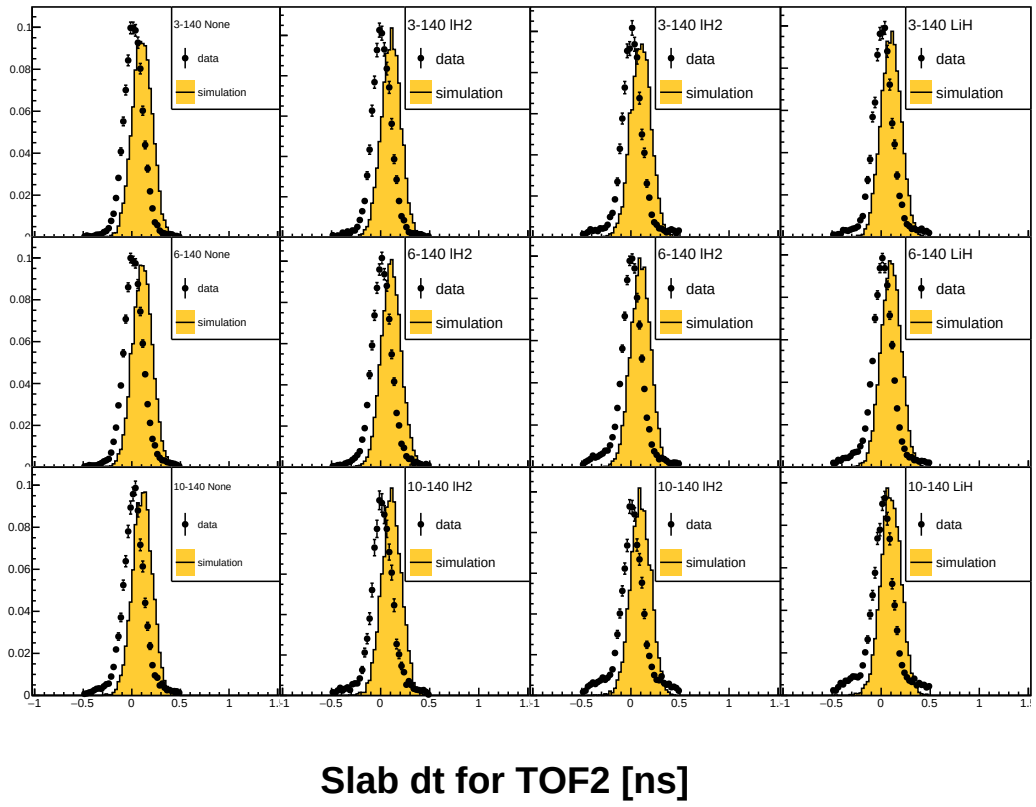

Figure 22: Measured time difference between adjacent TOF2 slabs for events in the downstream sample that make a slab hit.

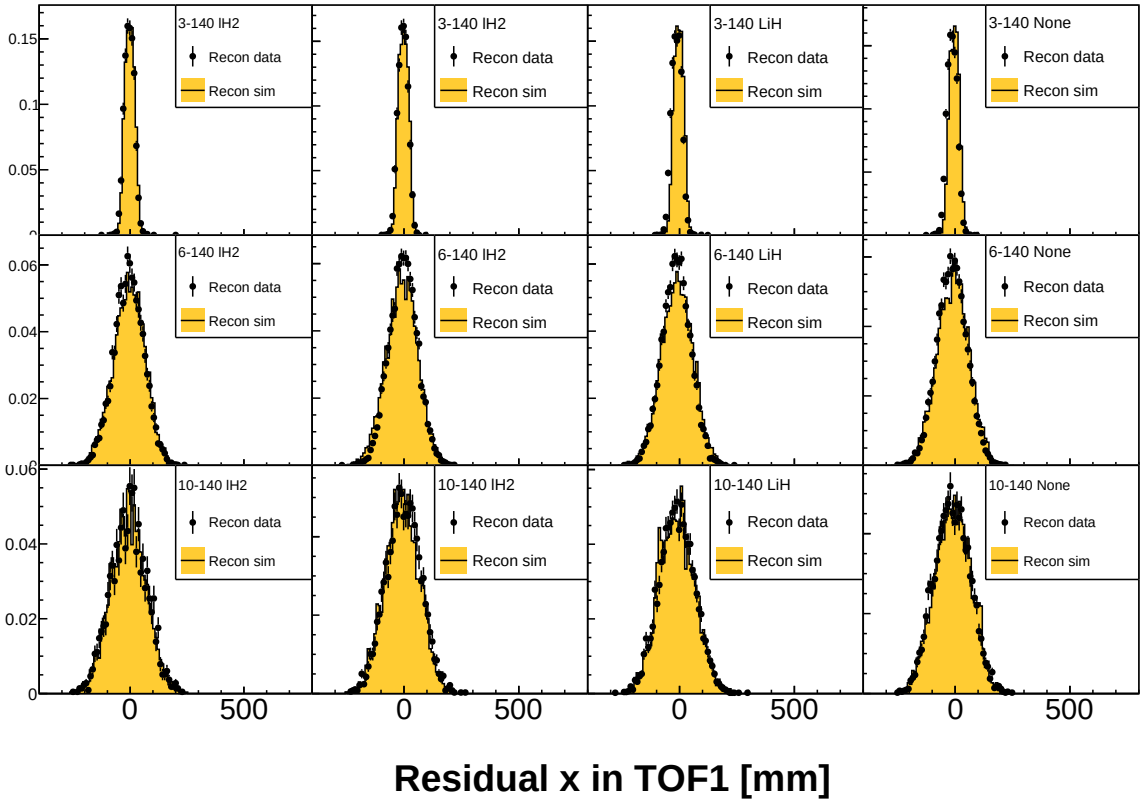

Figure 23: Residual horizontal (x) position in TOF1 of tracker tracks following extrapolation from TKU.

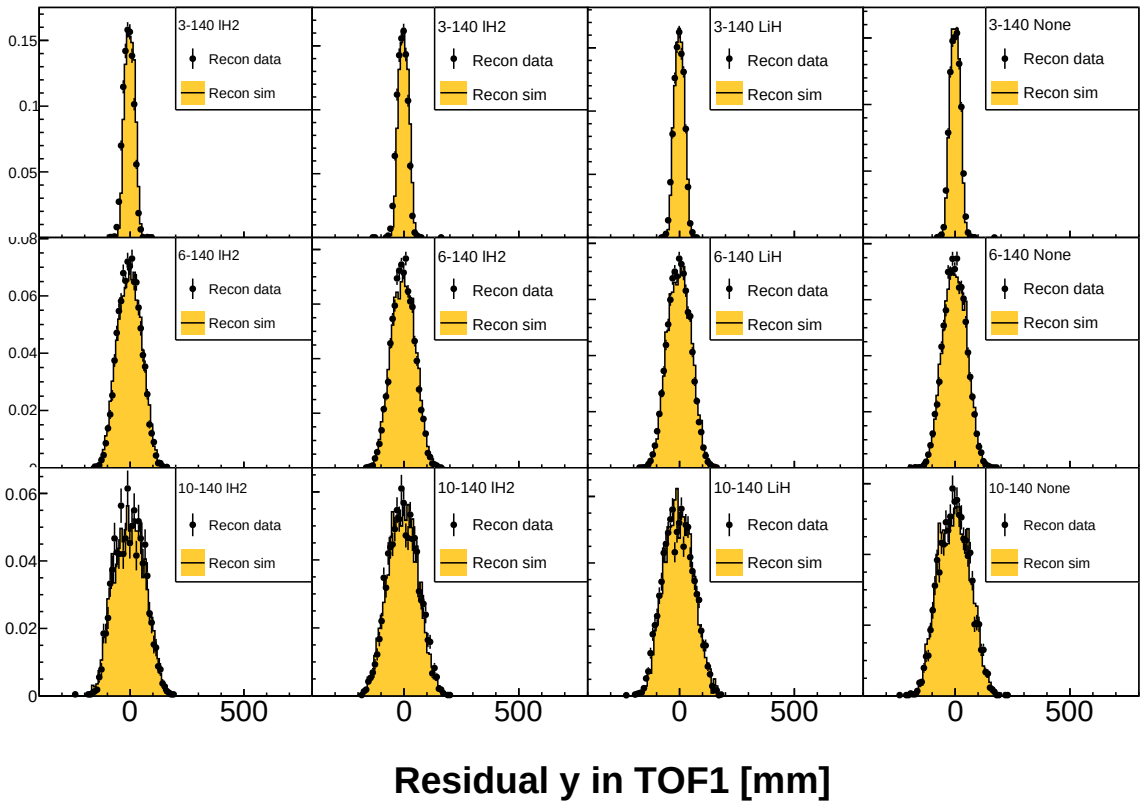

Figure 24: Residual vertical (y) position in TOF1 of tracker tracks following extrapolation from TKU.

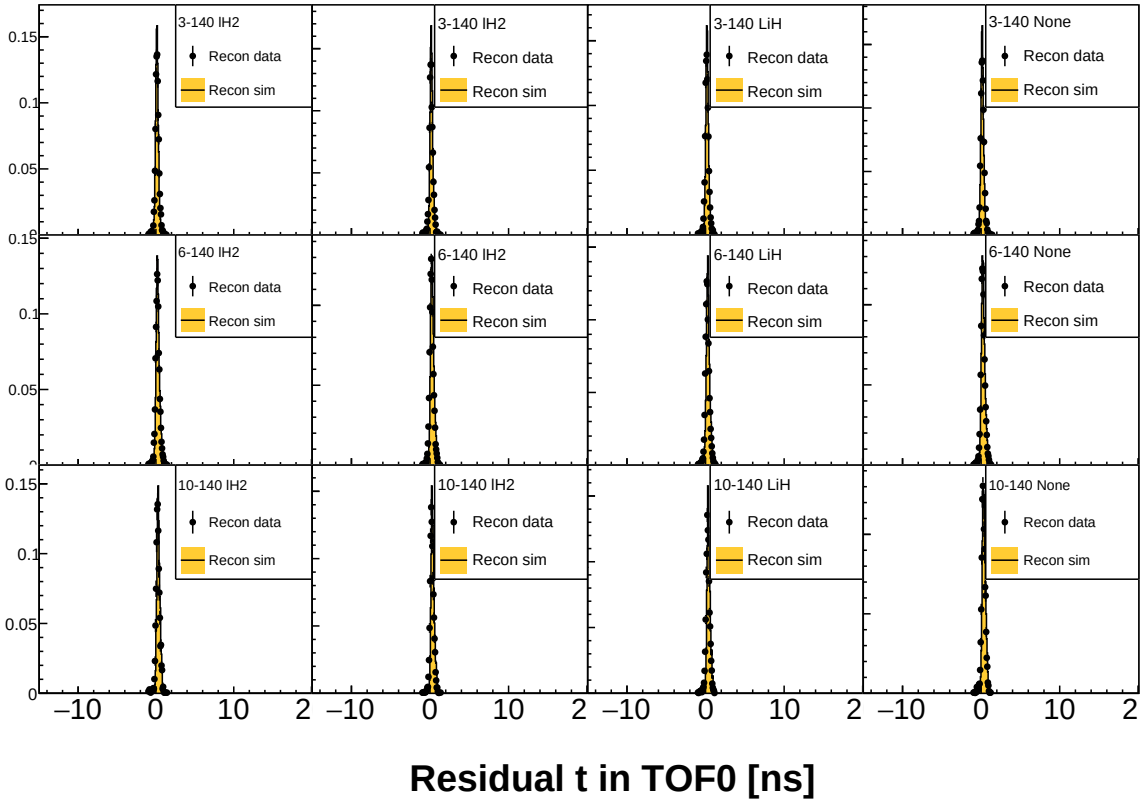

Figure 25: Residual TOF0 time of the extrapolated track. Track trajectories were drawn from TKU, while the track times were drawn from TOF1 with appropriate offsets for time-of-flight from TKU to TOF1 considered.

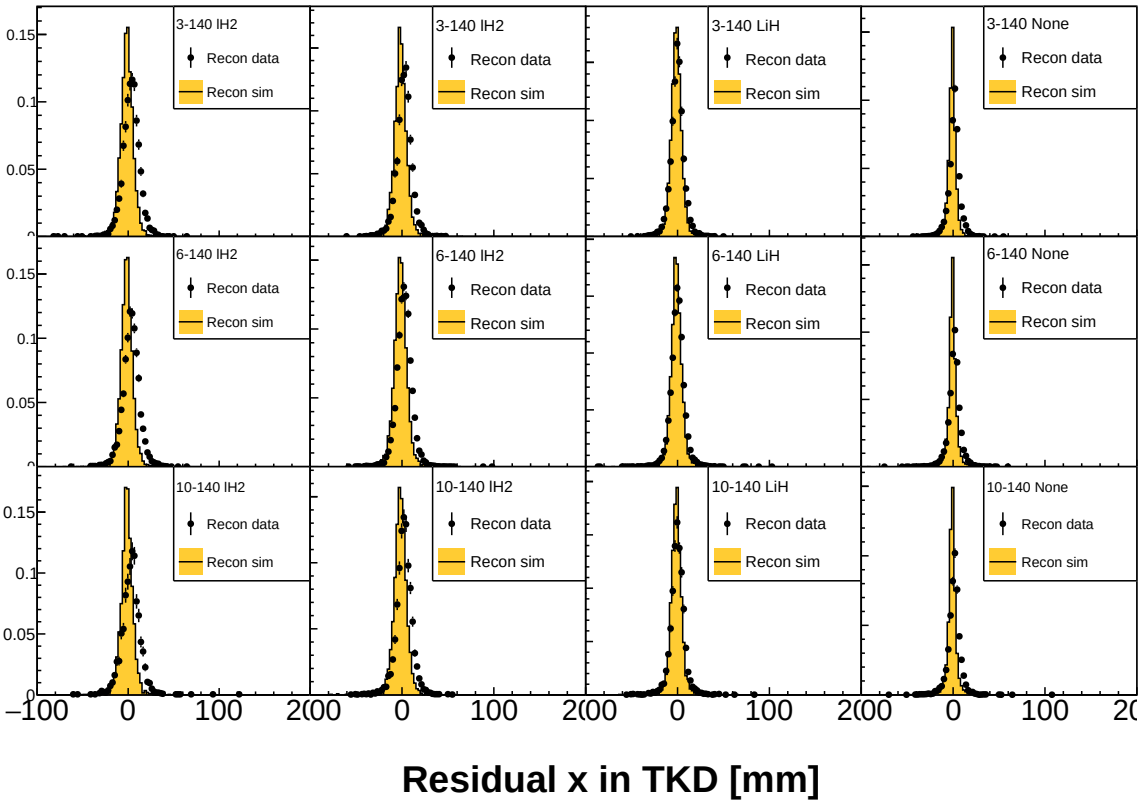

Figure 26: TKD x position.

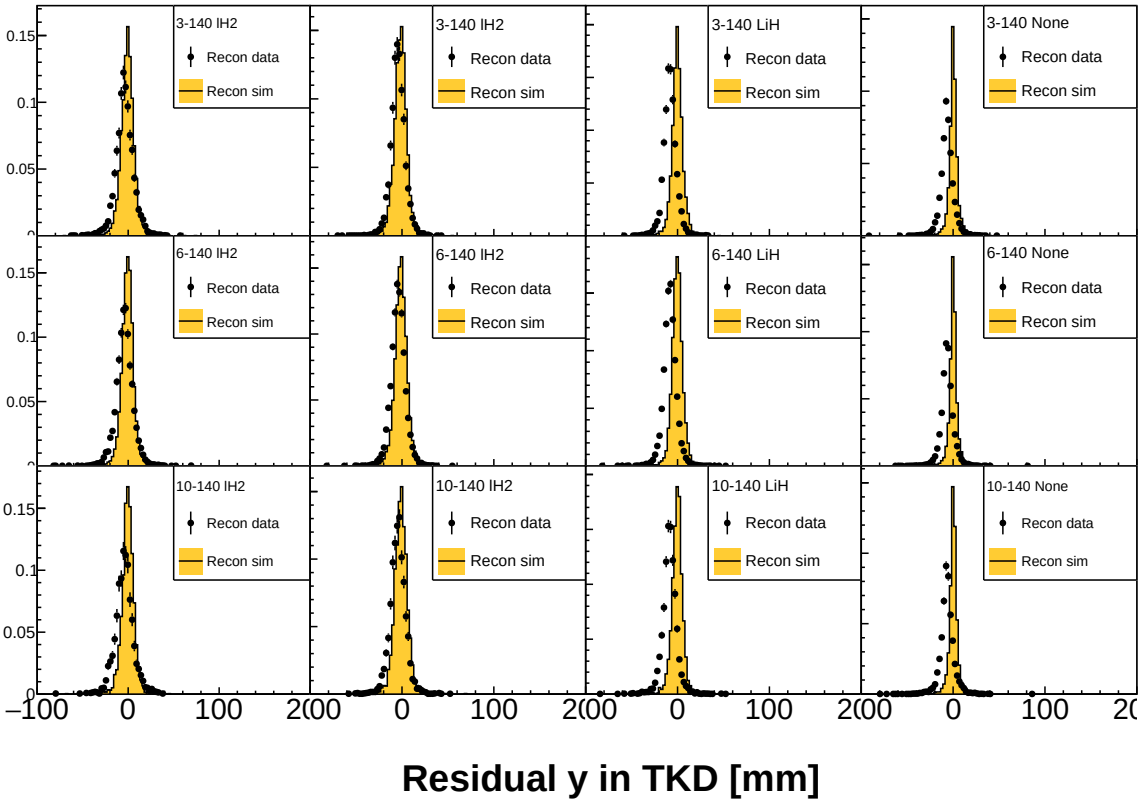

Figure 27: TKD y position.

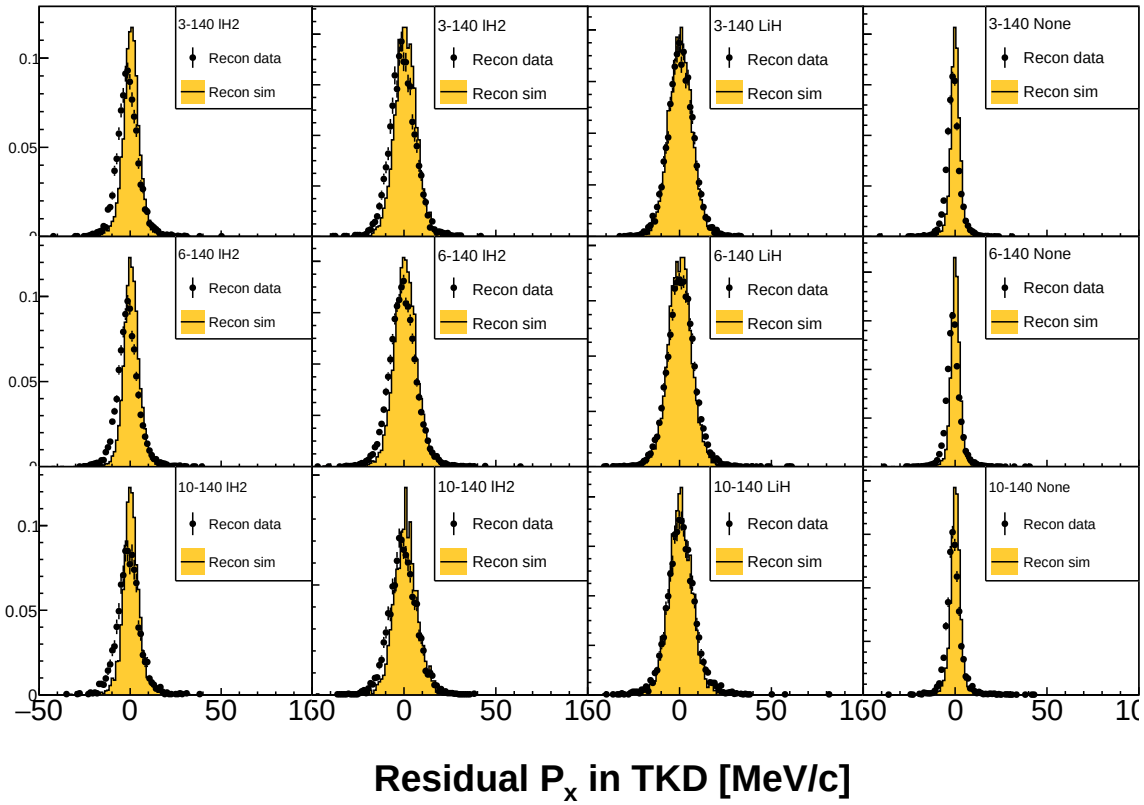

Figure 28: TKD py momentum.

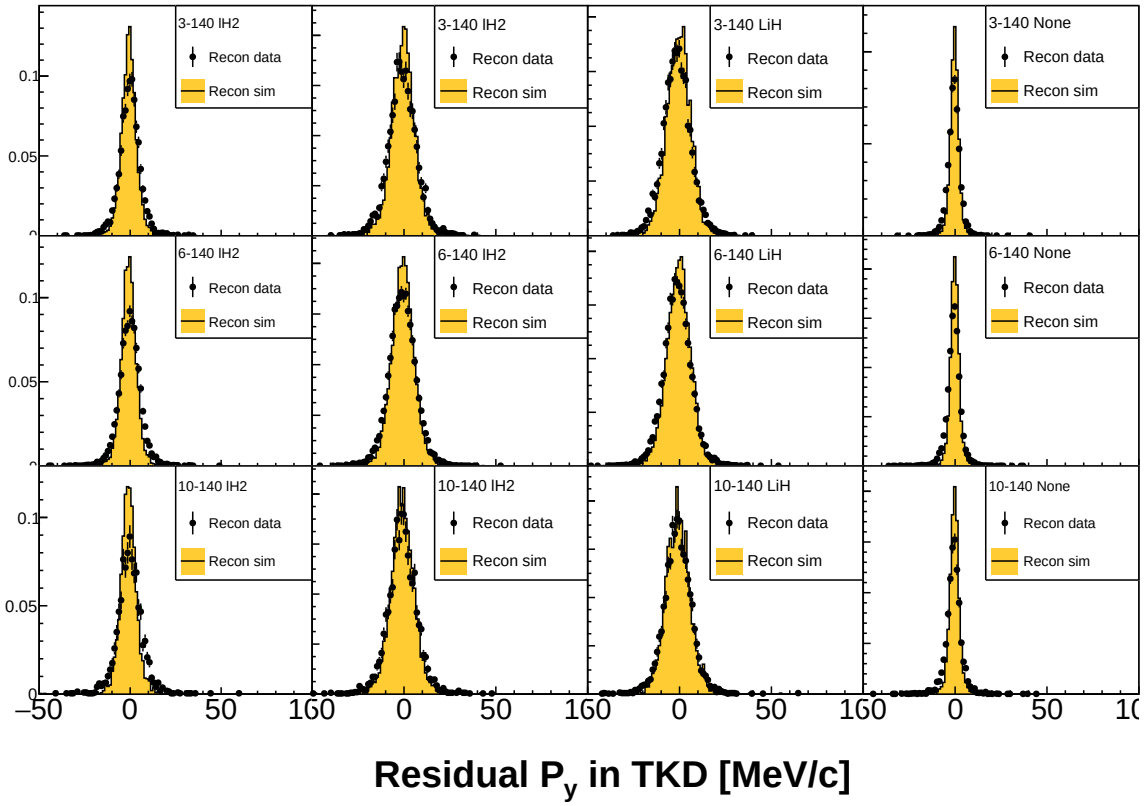

Figure 29: TKD px momentum.

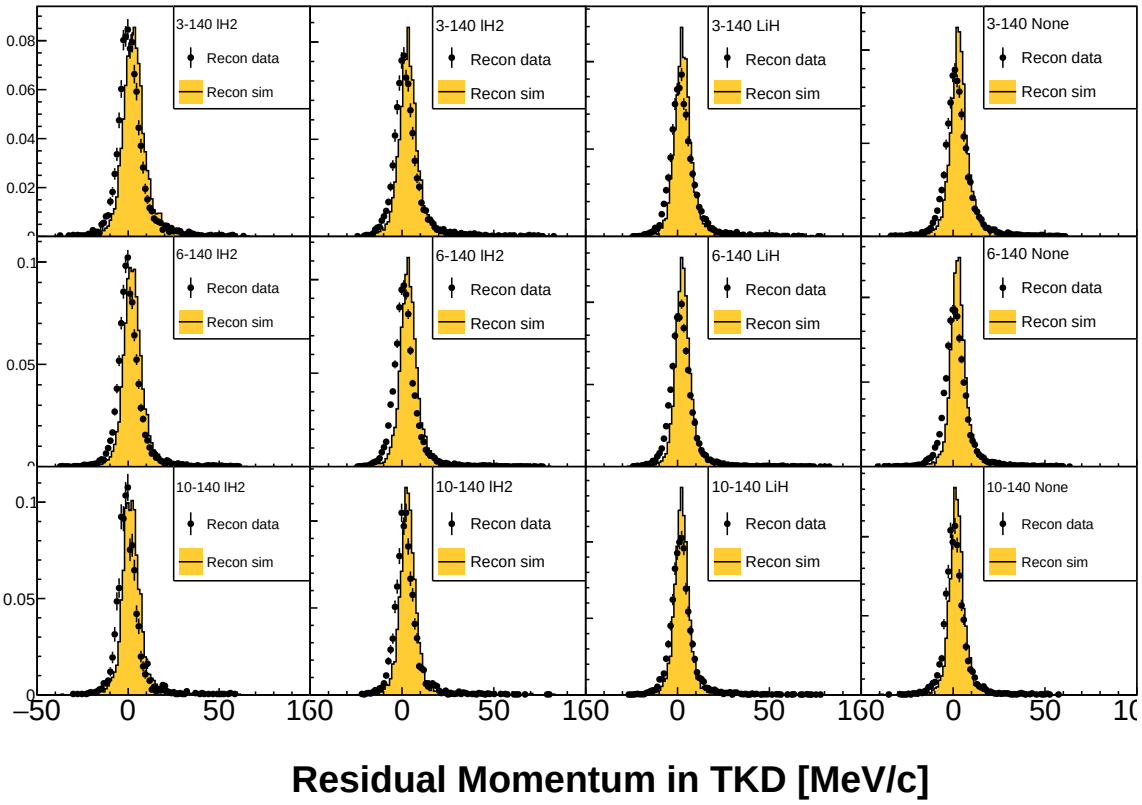

Figure 30: TKD total momentum.

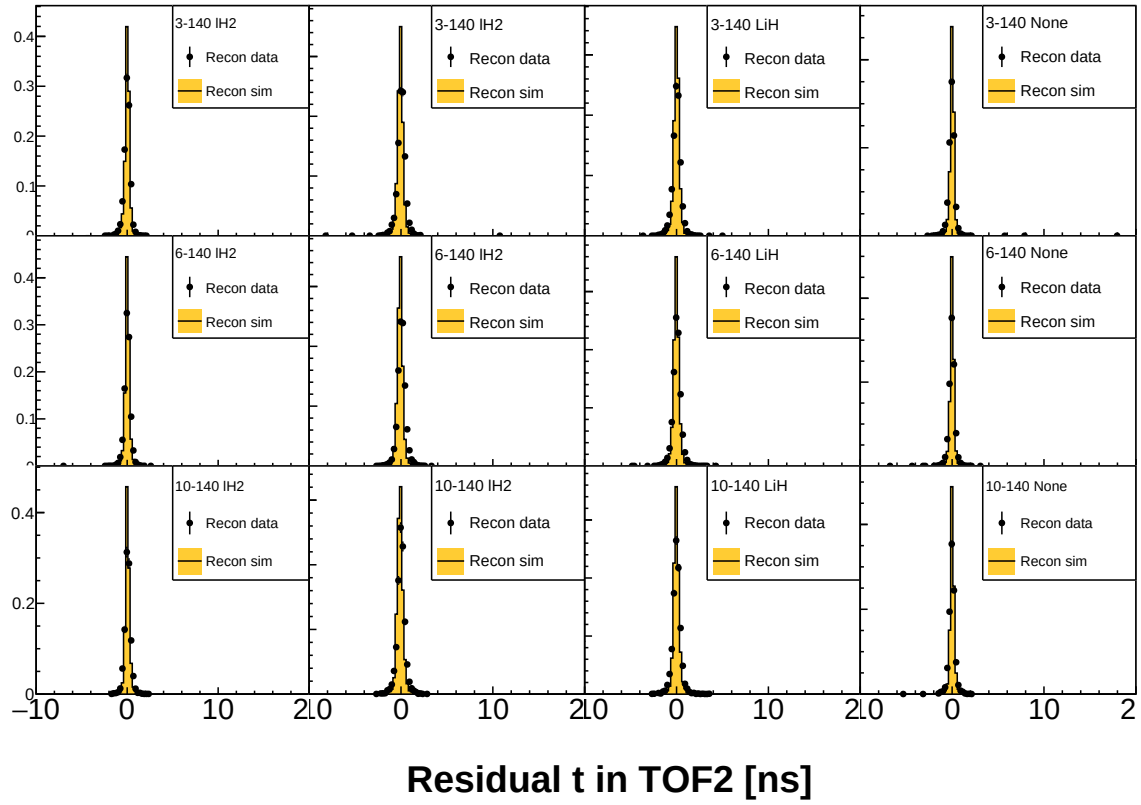

Figure 31: TOF2 time.

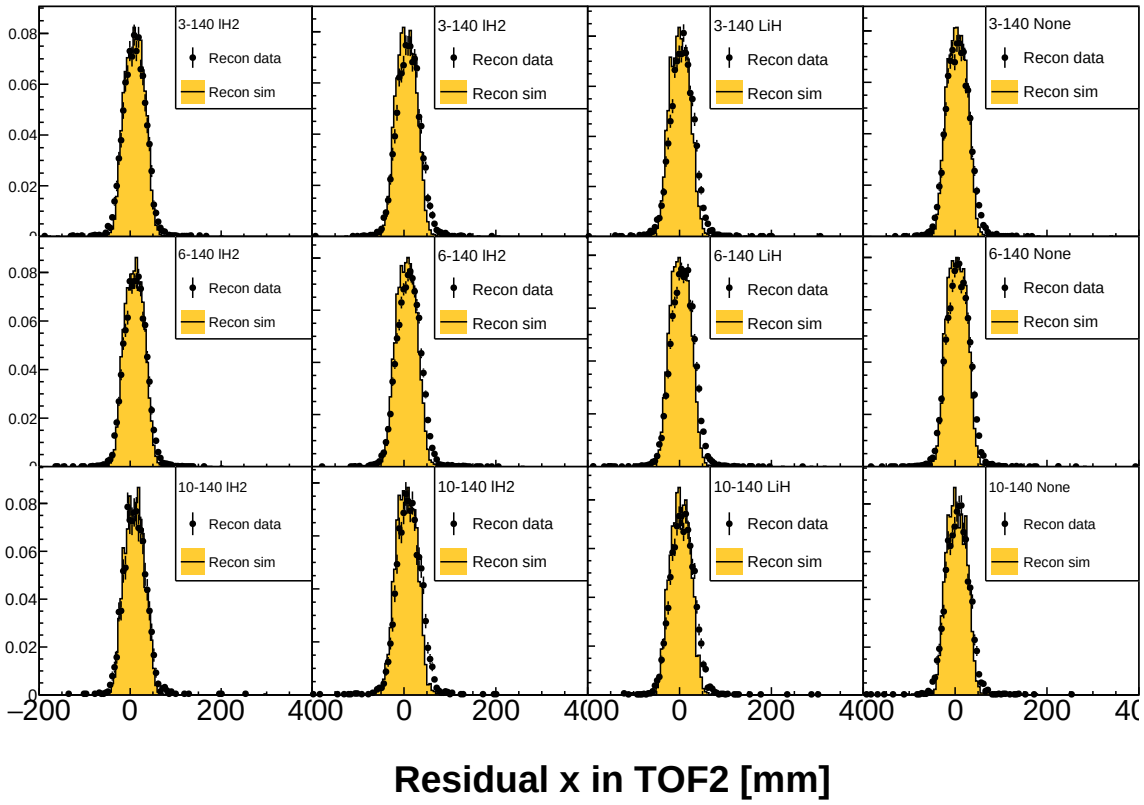

Figure 32: TOF2 x position.

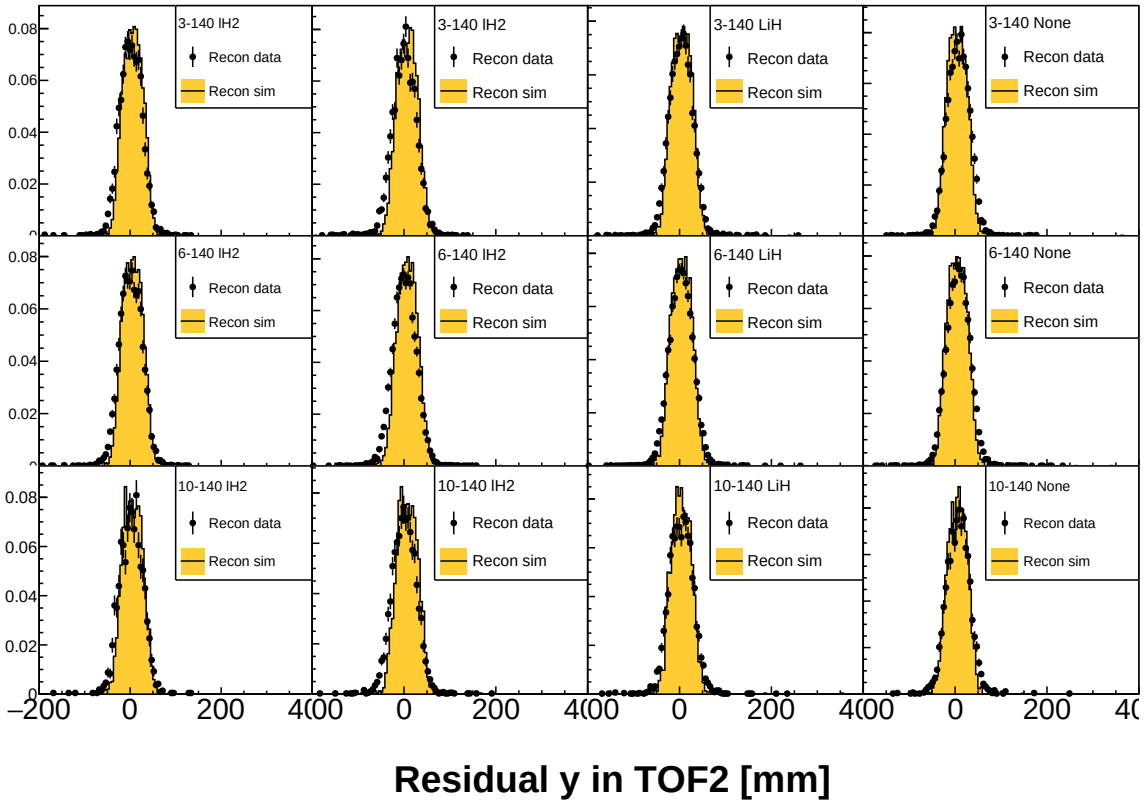

Figure 33: TOF2 y position.

7 Cooling Channel and Optics

Having validated the diagnostics, it is now of interest to examine the properties of the cooling channel.

7.1 Input Beam

The input beams into the cooling channel are expected to be consistent between different beamline settings, as the upstream cooling channel the

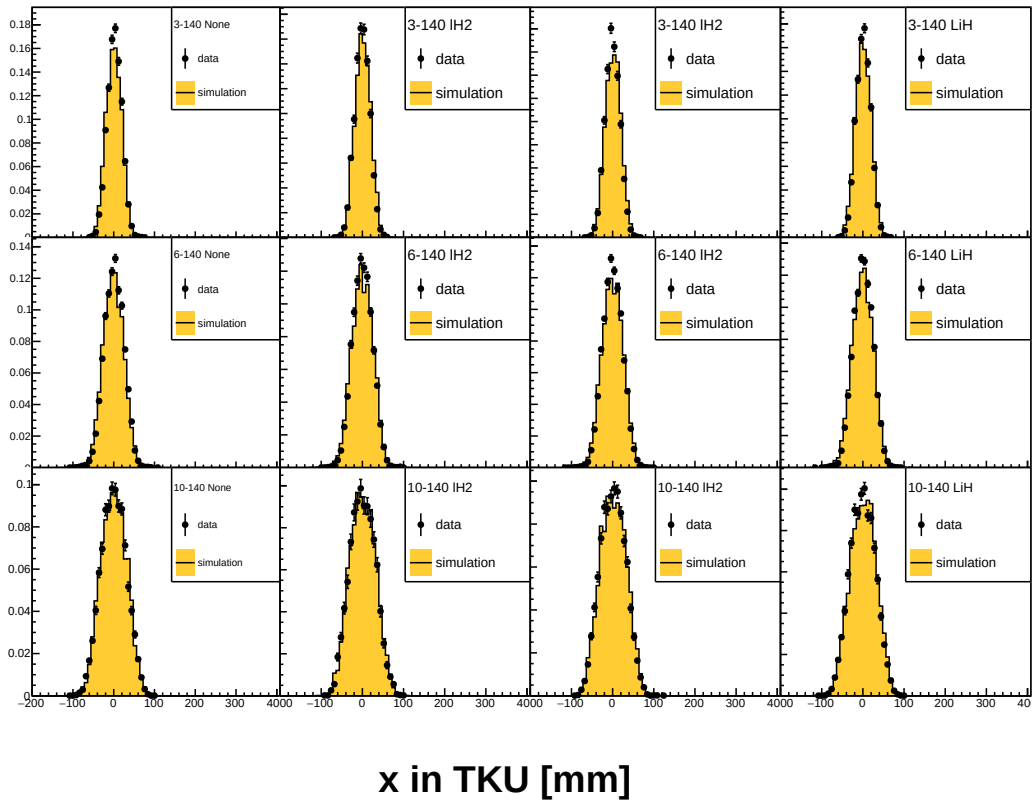

Figure 34: Horizontal position distribution in TKU for all events in the upstream sample.

7.2 Magnets

The MICE cooling channel consists of 12 coils arranged in 3 magnet assemblies, SSU, FC and SSD. As shown in fig. 15 the magnetic field is exceptionally reproducible, even over several weeks. As shown in fig. 15 the beam transport is exceptionally reproducible, even over several weeks.

Do I need to plot the currents as well?

7.3 Beam Transport

7.4 Absorber

Demonstrate that we understand the absorbers? Show that mean, RMS of extrapolated tracks is consistent with models for energy loss/straggling and MCS.

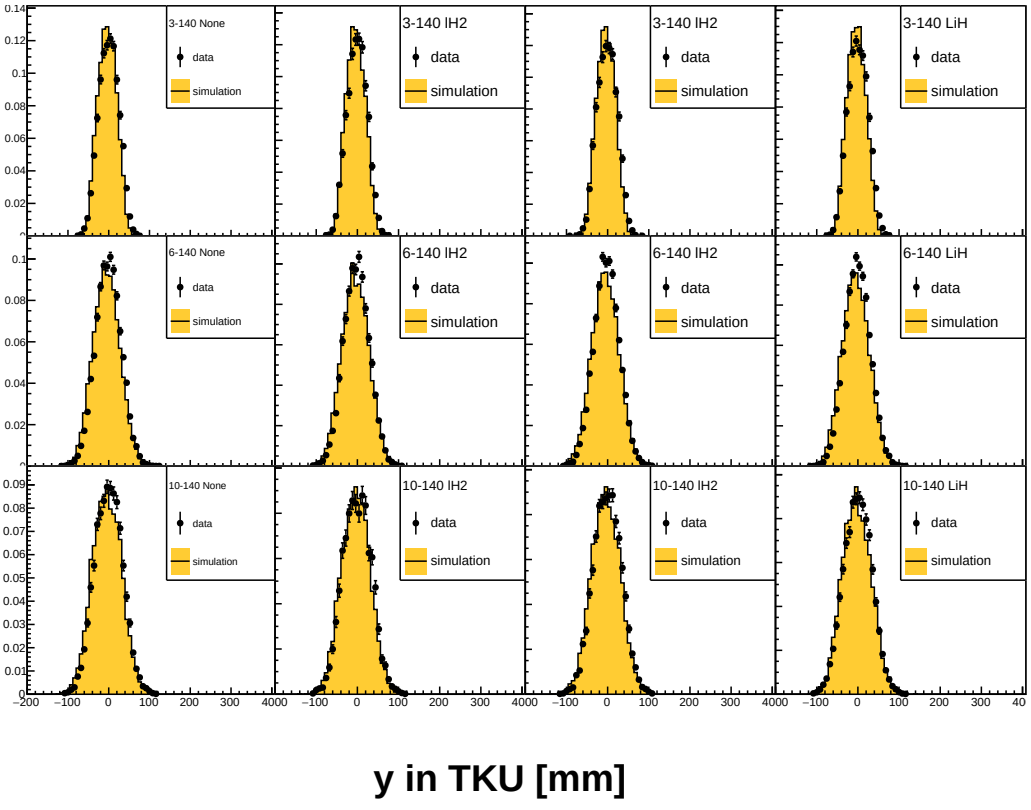

Figure 35: Vertical position distribution in TKU for all events in the upstream sample.

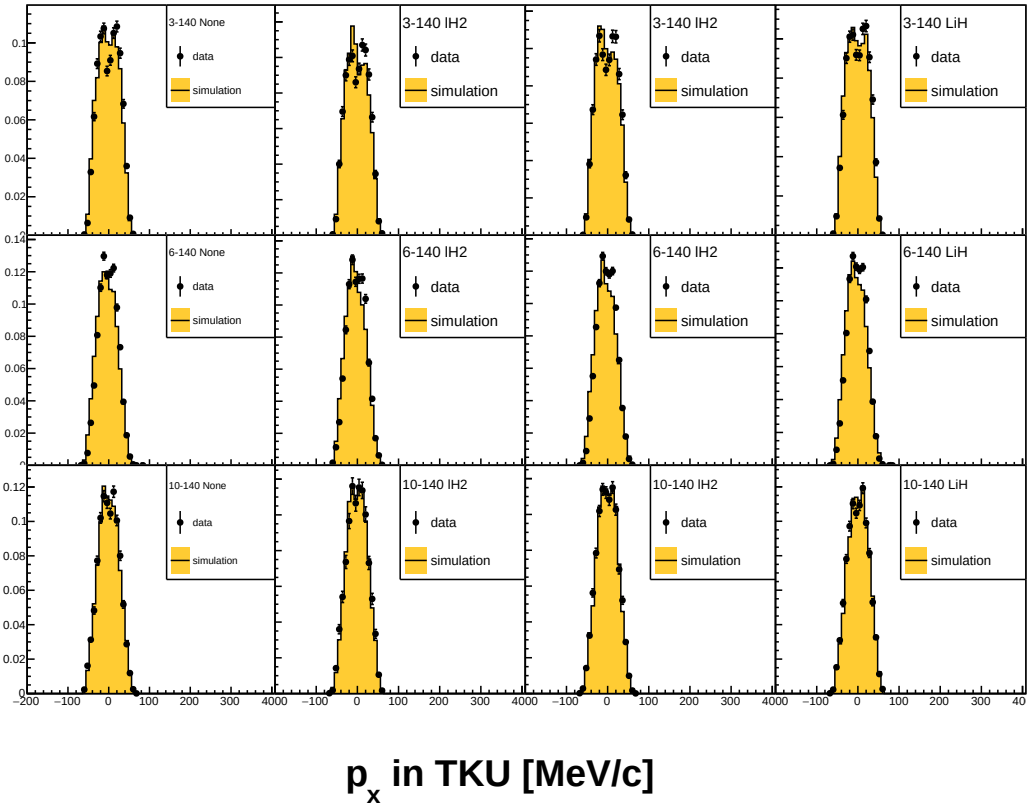

Figure 36: Horizontal momentum distribution in TKU for all events in the upstream sample.

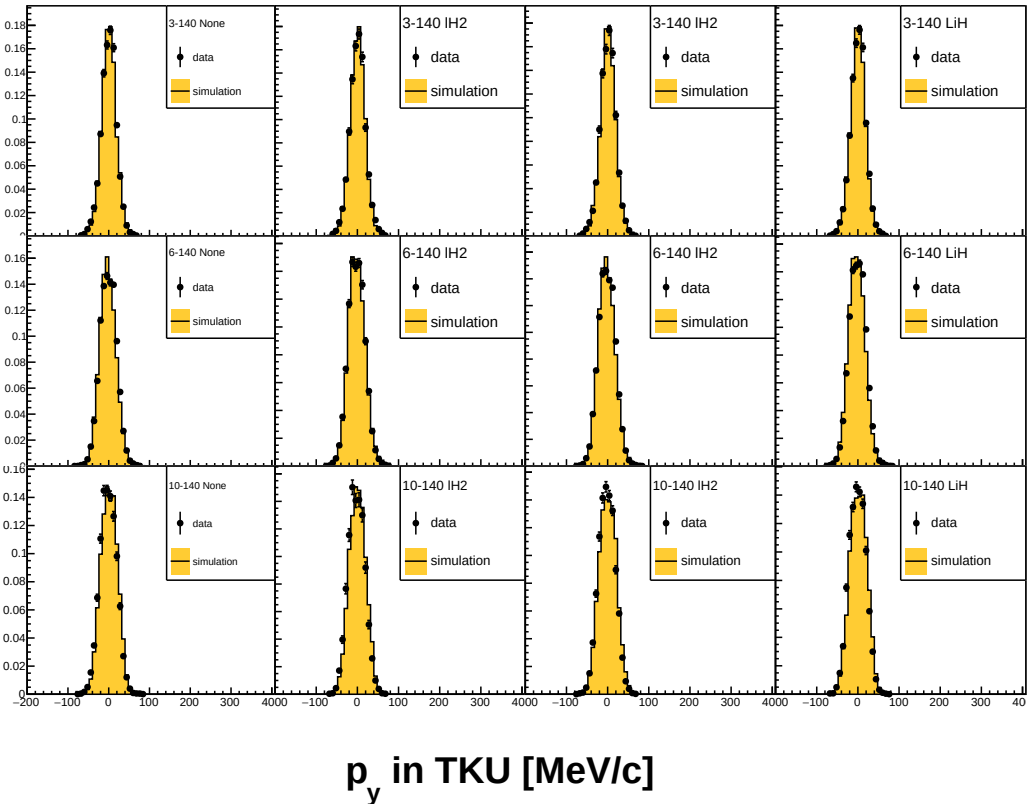

Figure 37: Vertical momentum distribution in TKU for all events in the upstream sample.

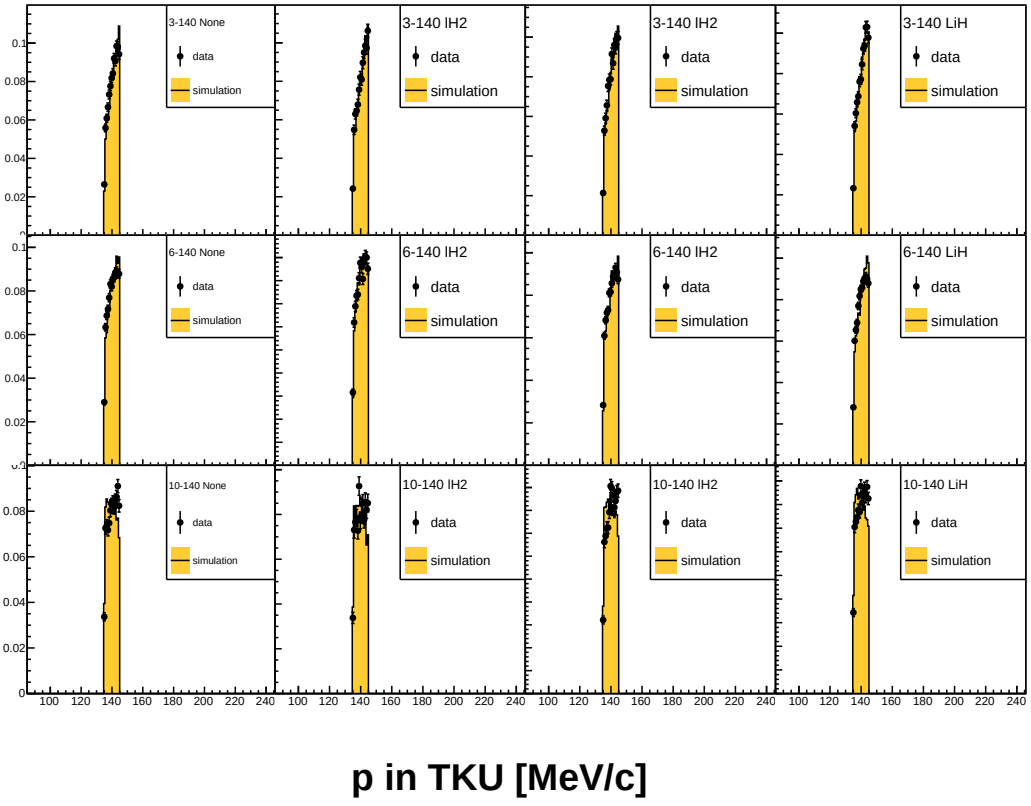

Figure 38: Total momentum distribution in TKU for all events in the upstream sample.

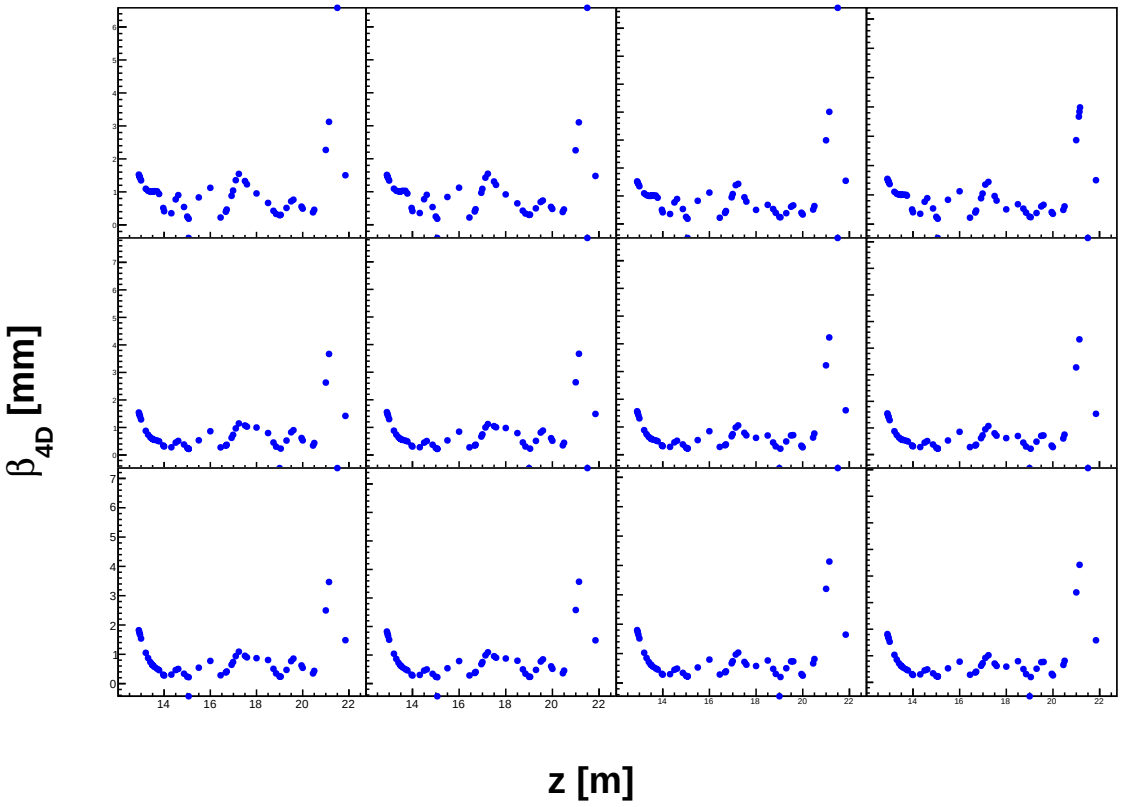

Figure 39: β_{4D} for events in the downstream sample, measured in TKU and extrapolated downstream (blue points) and events in TKD extrapolated downstream (red points).

7.5 Output Beam

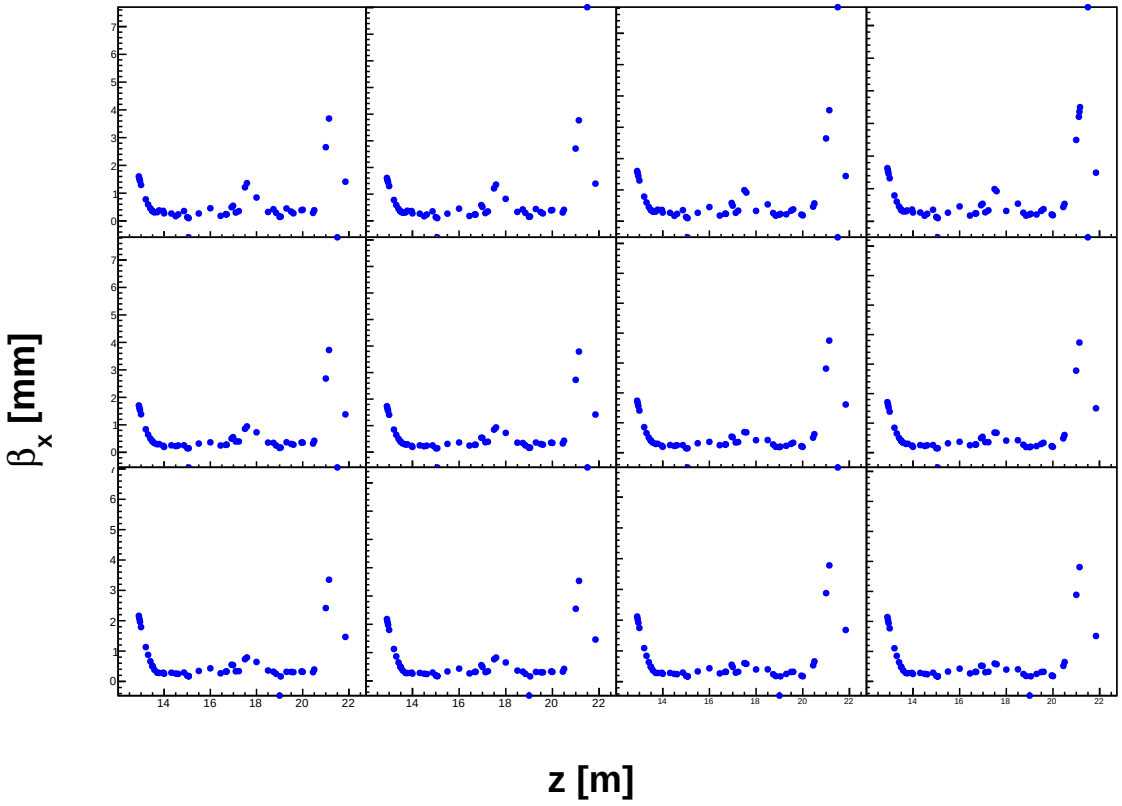

Figure 40: β_x of events in the downstream sample, measured in TKU and extrapolated downstream (blue points) and events in TKD extrapolated downstream (red points).

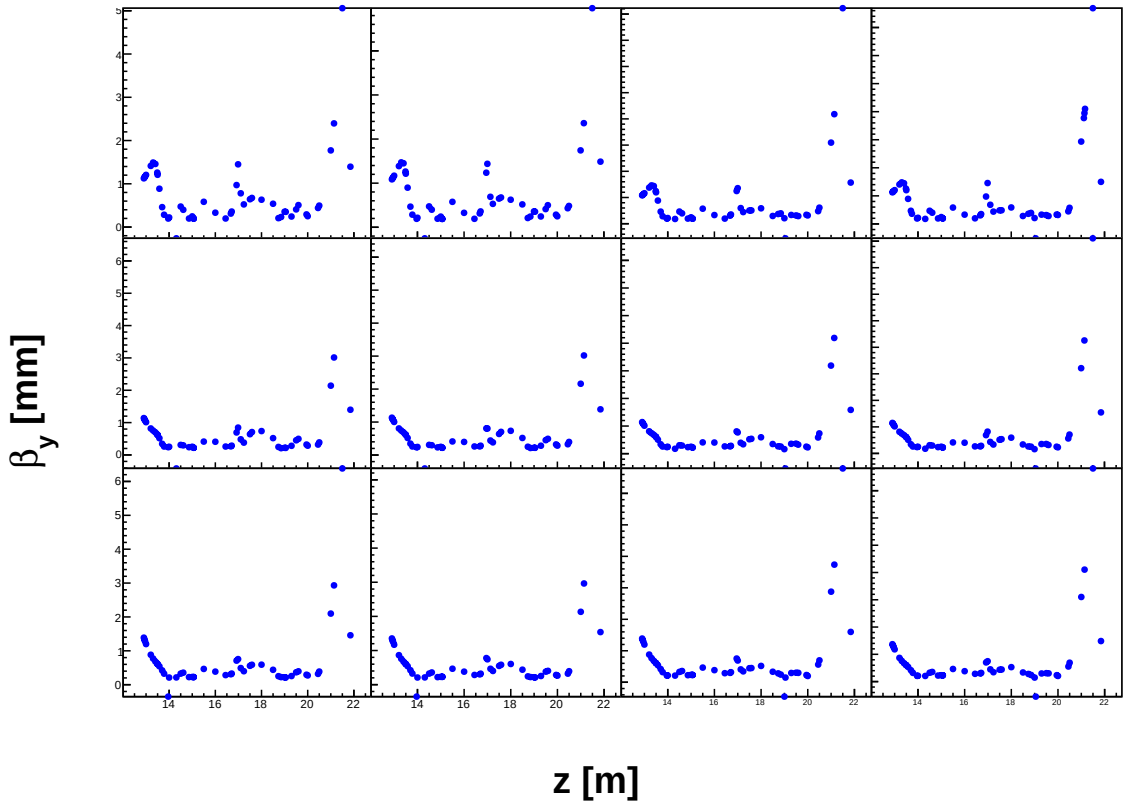

Figure 41: β_y of events in the downstream sample, measured in TKU and extrapolated downstream (blue points) and events in TKD extrapolated downstream (red points).

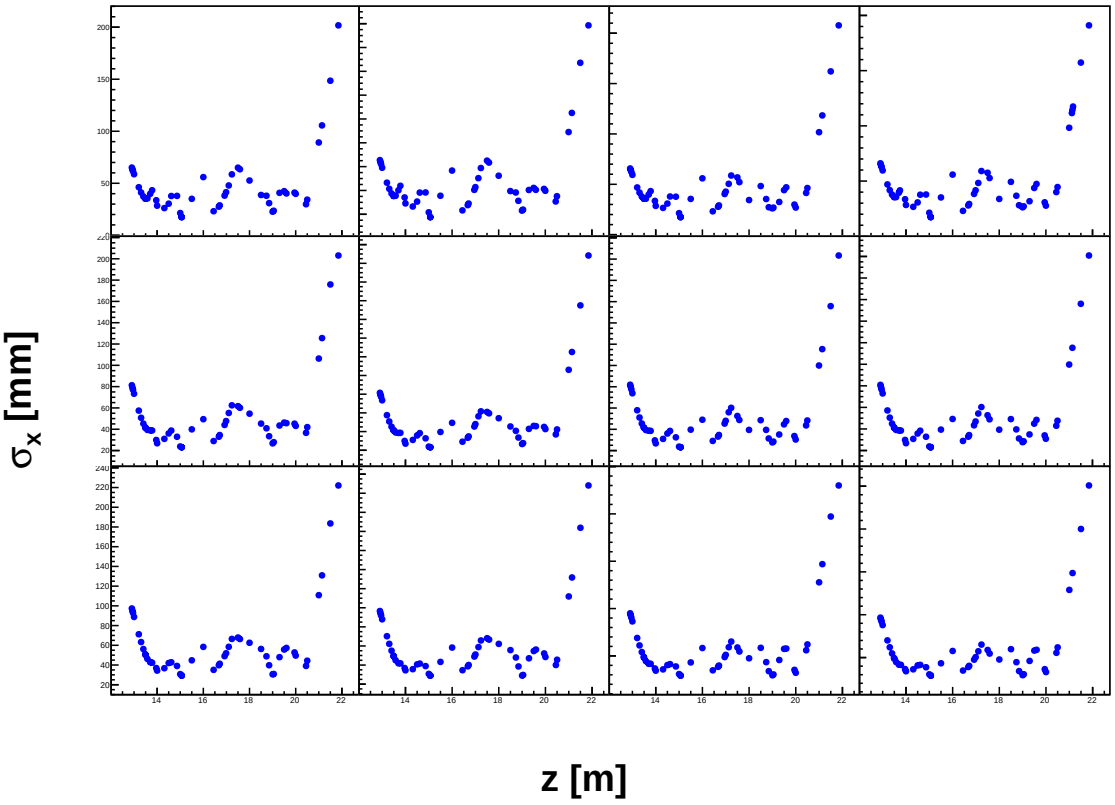

Figure 42: Standard deviation of the vertical beam positions, σ_x, for events in the downstream sample, measured in TKU and extrapolated downstream (blue points) and events in TKD extrapolated downstream (red points).

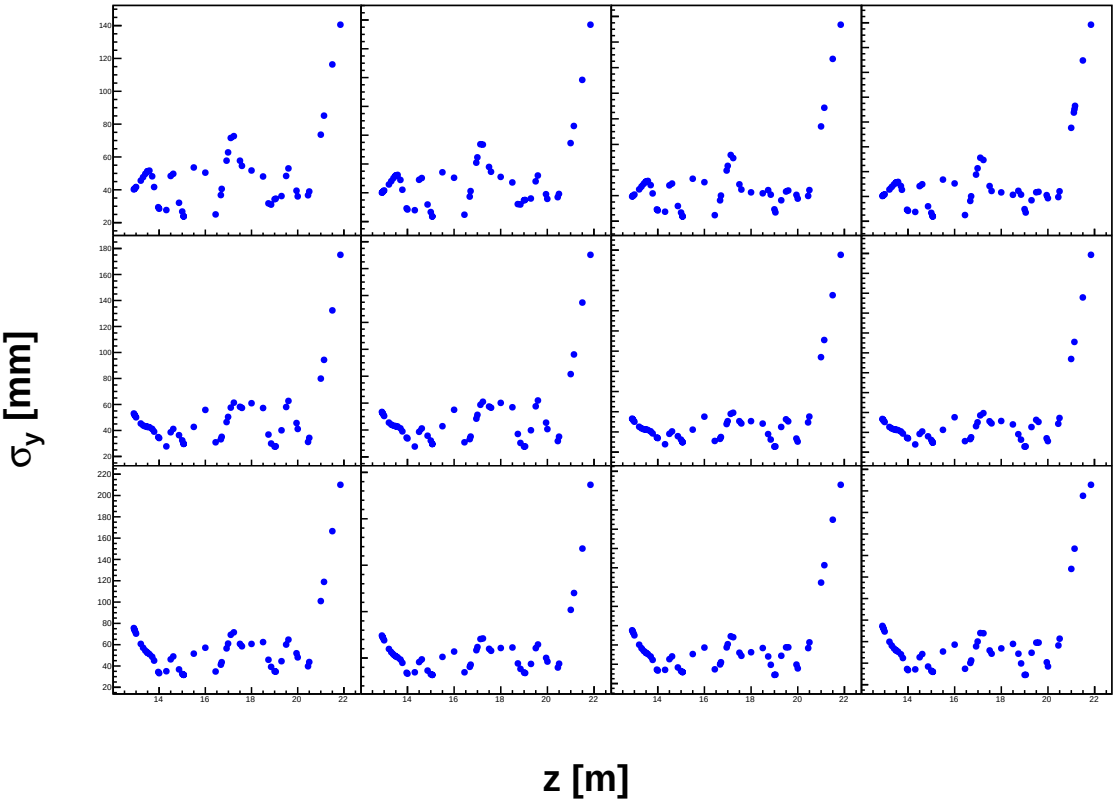

Figure 43: Standard deviation of the vertical beam positions, σ_y, for events in the downstream sample, measured in TKU and extrapolated downstream (blue points) and events in TKD extrapolated downstream (red points).

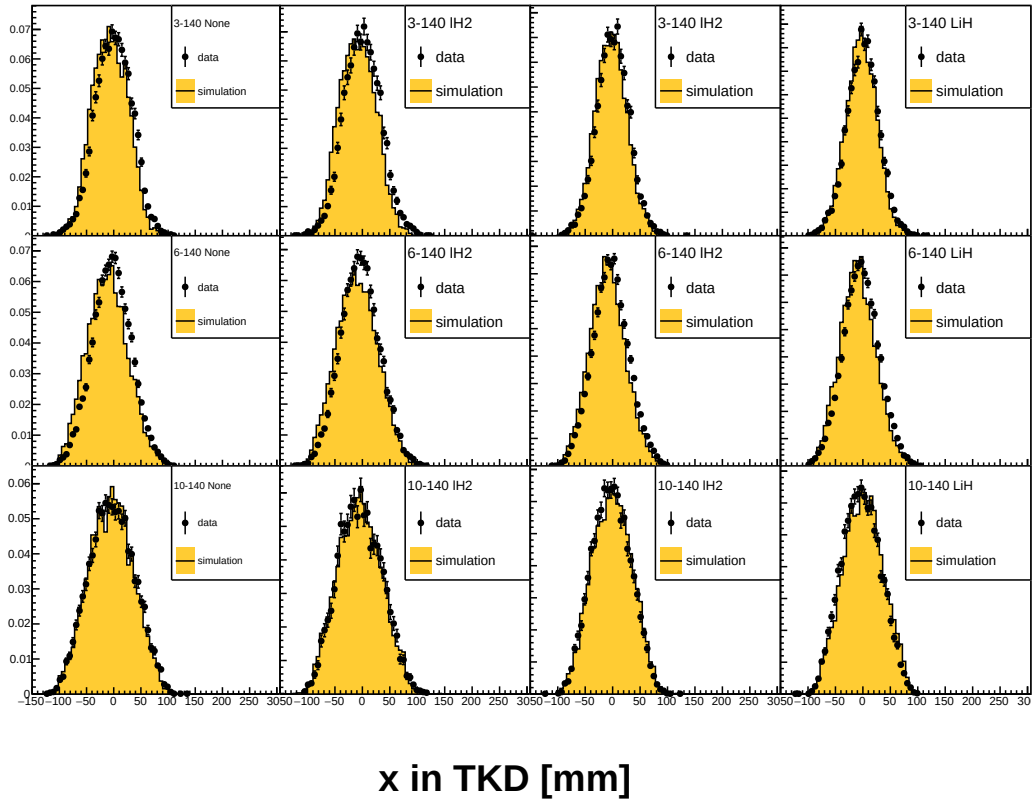

Figure 44: Horizontal position distribution in TKD for all events in the downstream sample.

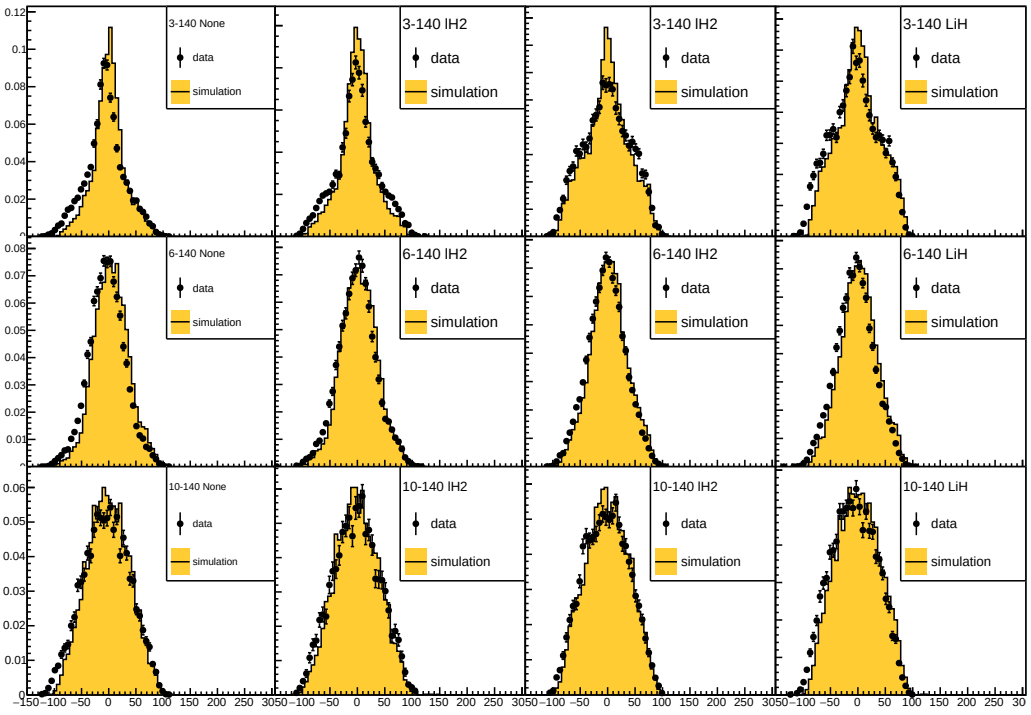

Figure 45: Vertical position distribution in TKD for all events in the downstream sample.

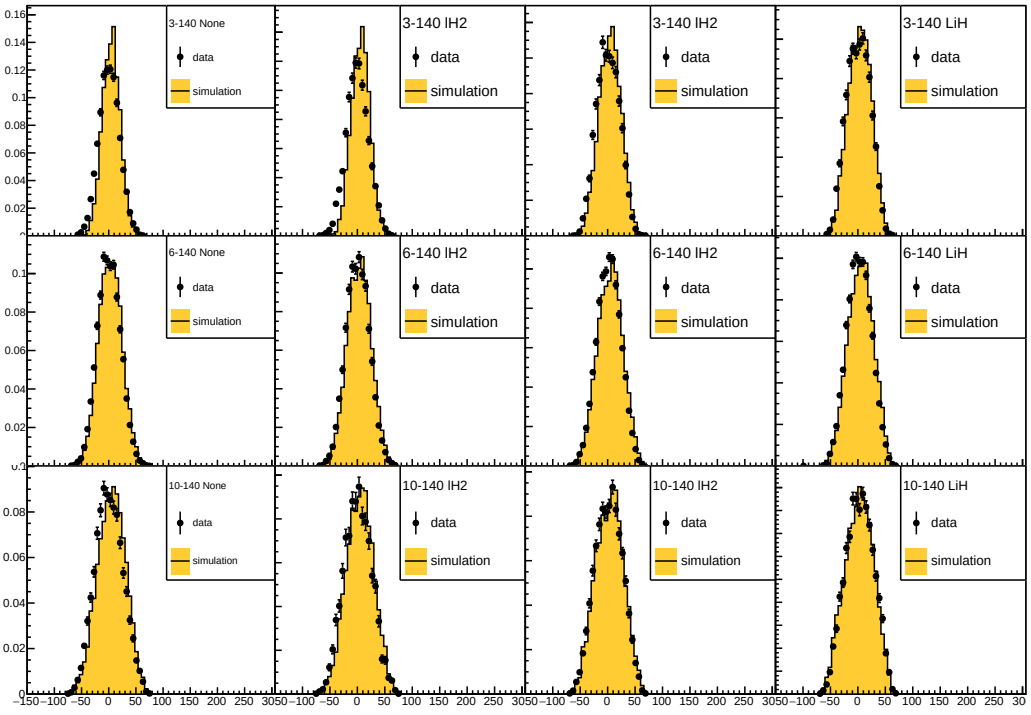

Figure 46: Horizontal momentum distribution in TKD for all events in the downstream sample.

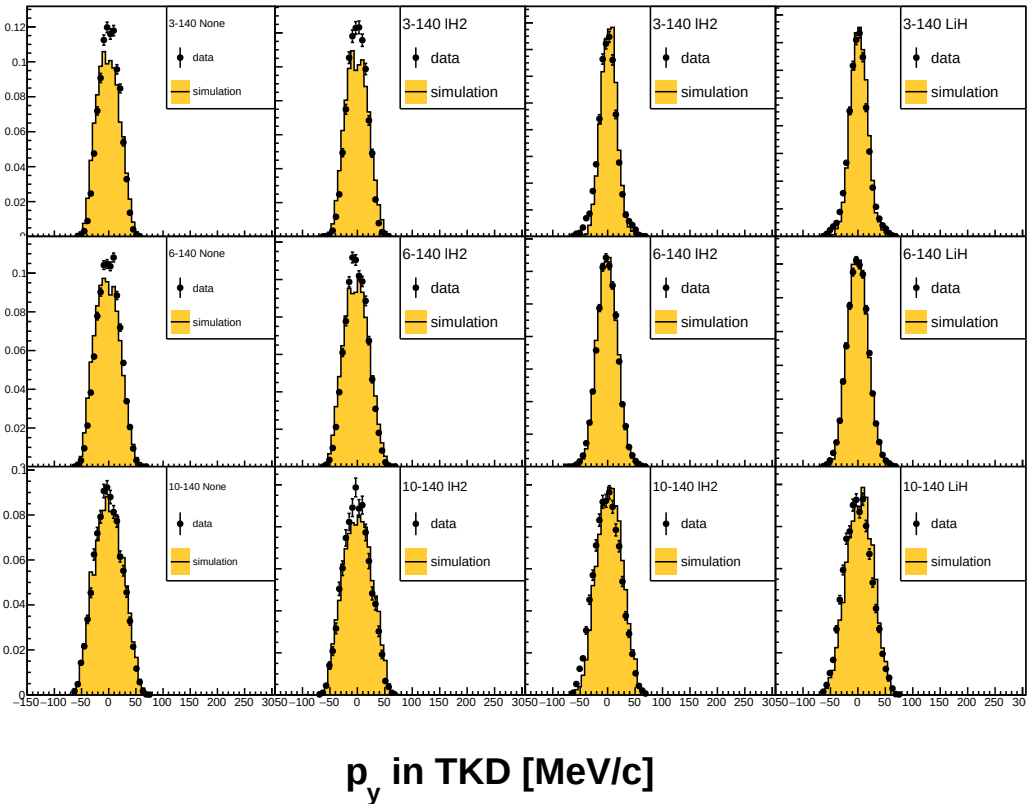

Figure 47: Vertical momentum distribution in TKD for all events in the downstream sample.

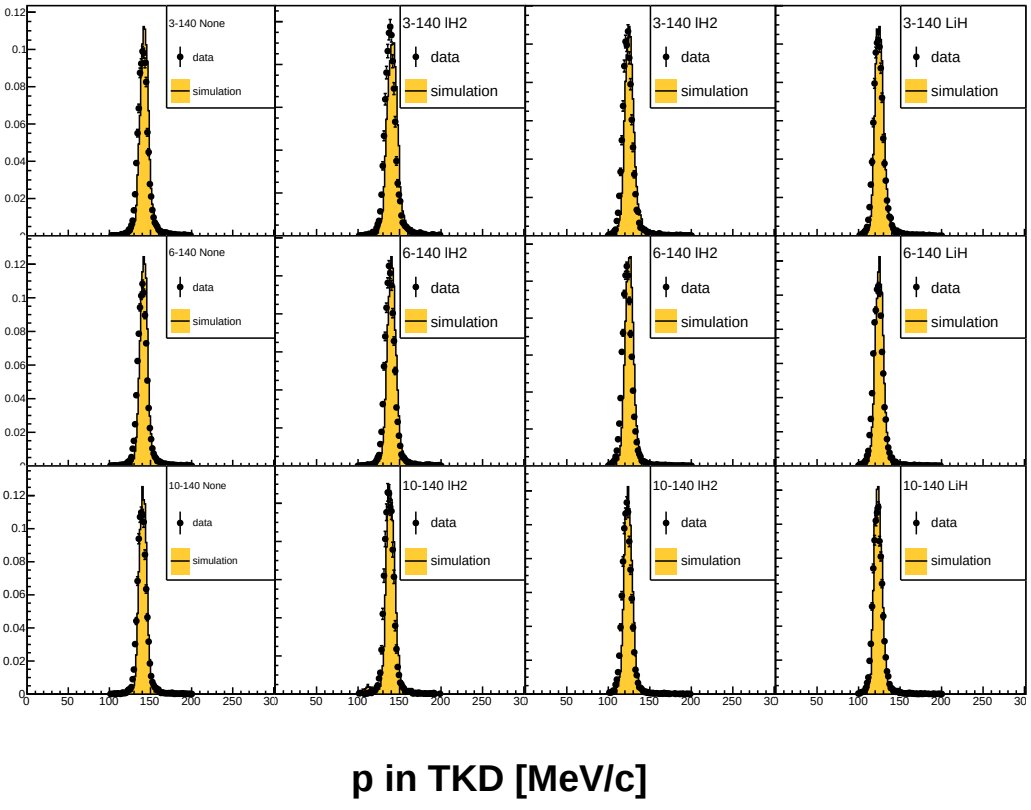

Figure 48: Total momentum distribution in TKD for all events in the downstream sample.

8 Results

Author Rogers

Describe the results.

Define amplitude.

8.1 Amplitude Distribution

The change in number of events upstream and downstream of the absorber is shown in **??** for empty and full configurations.

Show amplitude distribution upstream vs amplitude downstream.

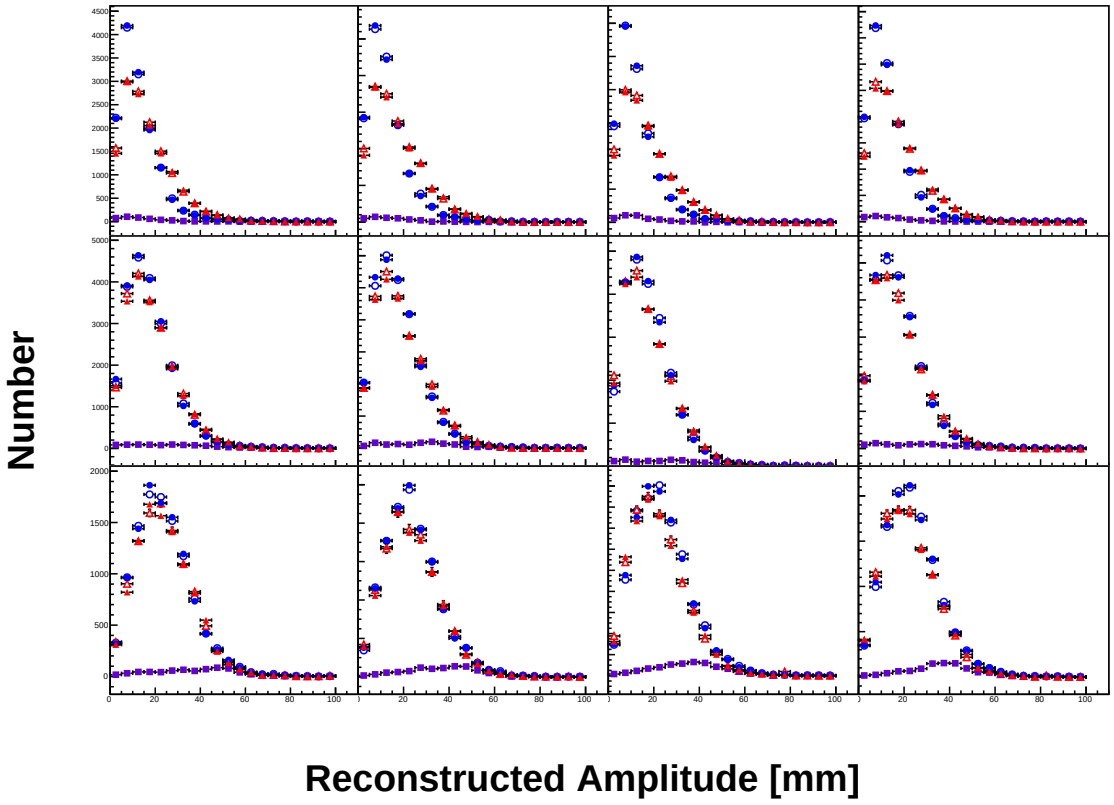

Figure 49: Amplitude PDF.

8.2 Corrections

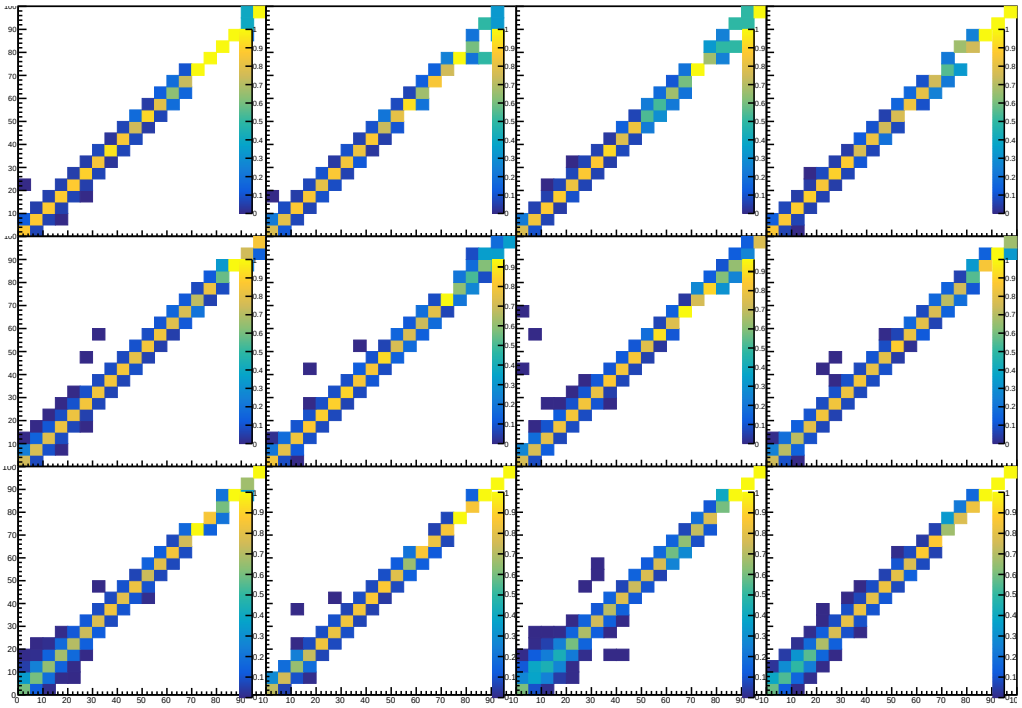

Figure 50: Migration matrix in TKU recon to recon truth (simulated).

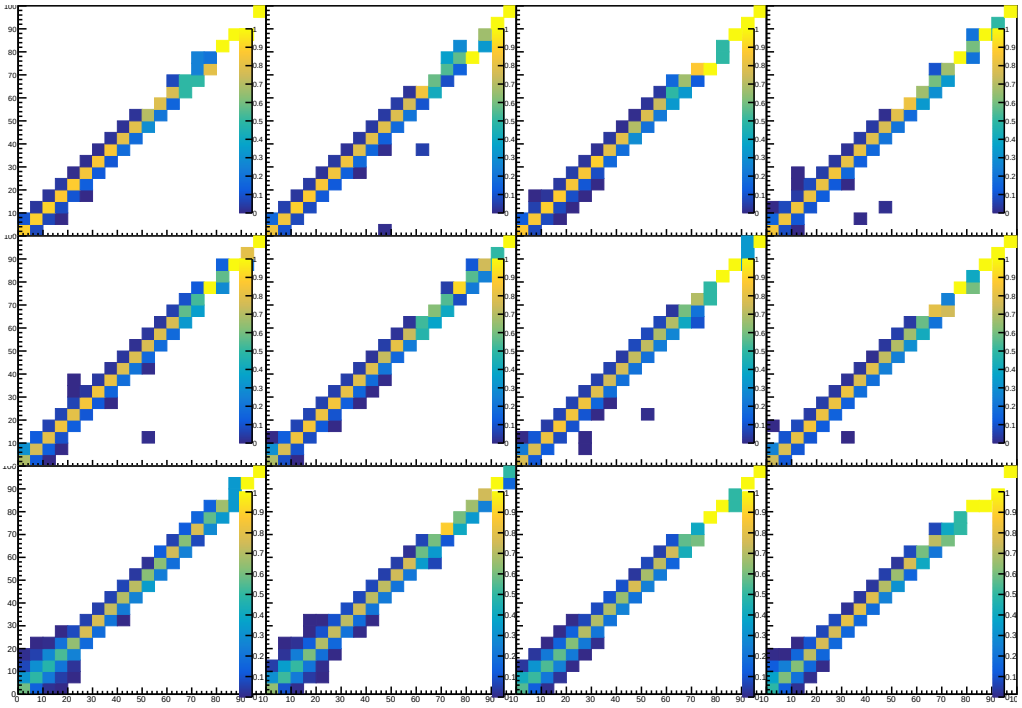

Figure 51: Migration matrix in TKD recon to recon truth (simulated).

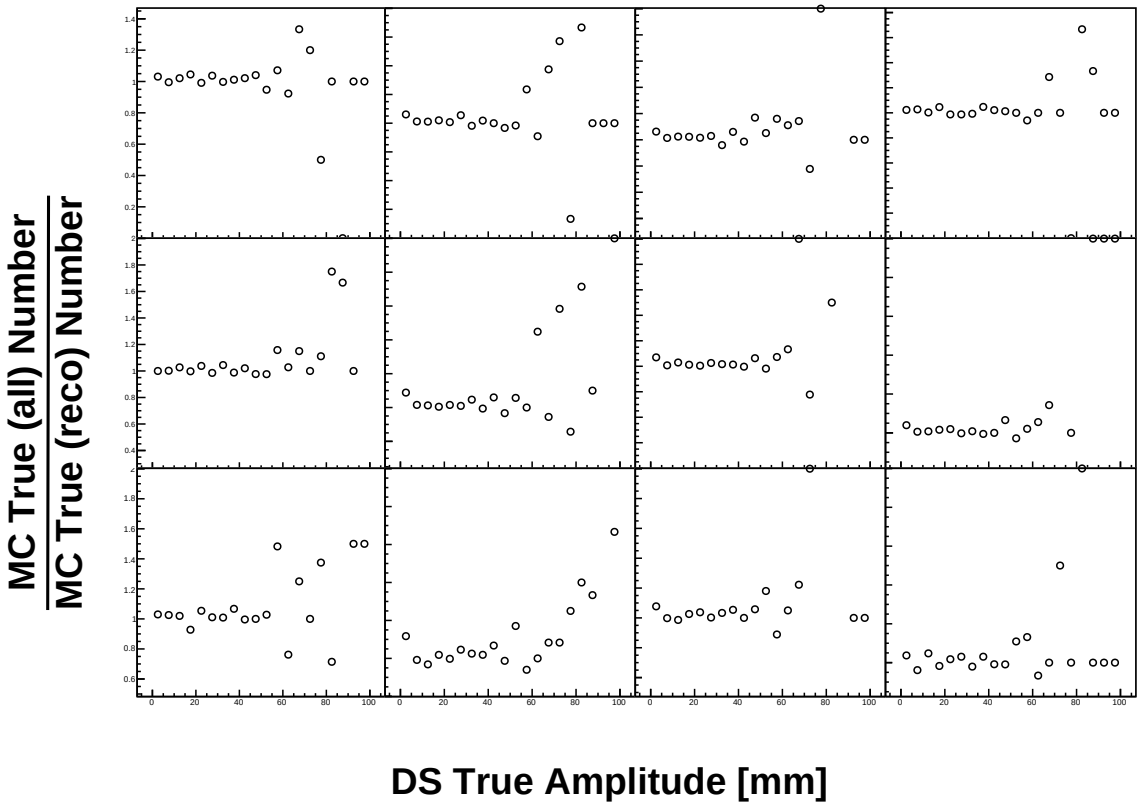

Figure 52: Impurity and inefficiency combined in TKD (simulated).

8.3 Presentation of results

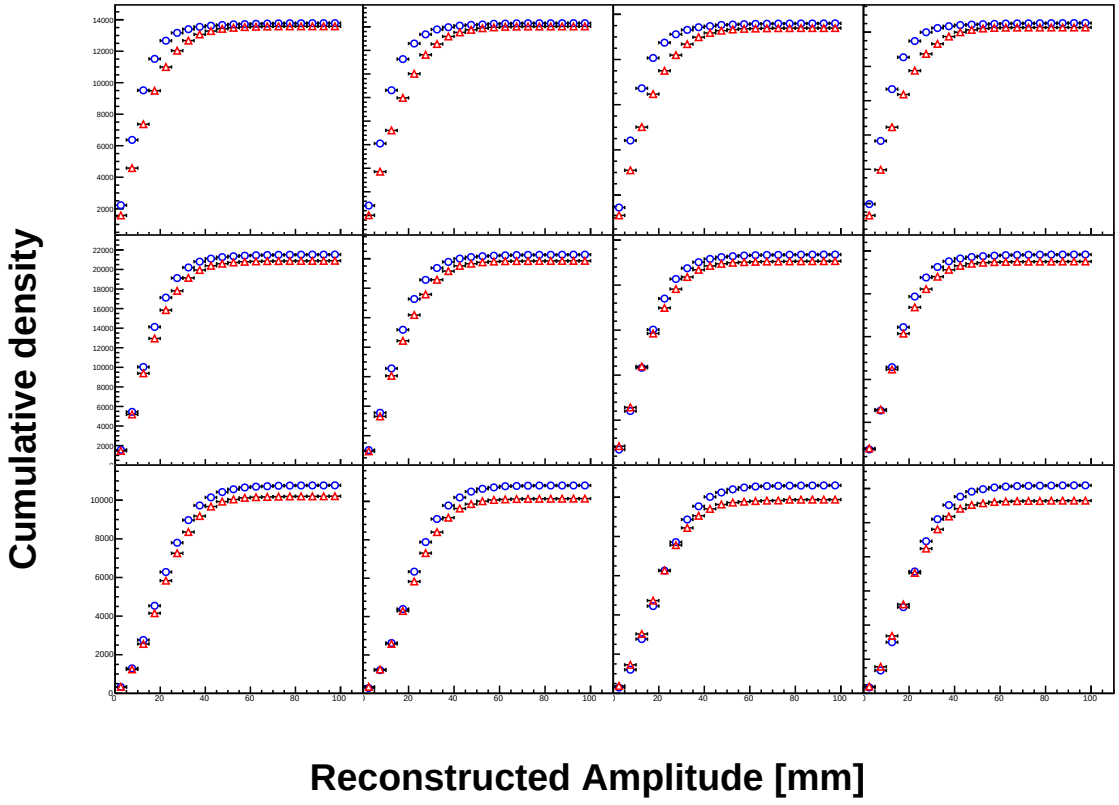

Figure 53: Amplitude Cumulative Density Function.

9 Uncertainties

Discuss how we deal with various uncertainties. I imagine two classes of uncertainty: (i) those that affect the measurement; (ii) those that affect the model.

9.1 Measurement Uncertainties

author: Rogers

The actual resolutions/etc have been introduced in the detectors section - so the job here is to make statistical/MC arguments about how they tie in to the data. E.g. how does TKD inefficiency affect emittance calculation?

- Detector resolution
- Detector noise and efficiency
- Magnetic field in reconstruction region

9.2 Model Uncertainties

author: Liu

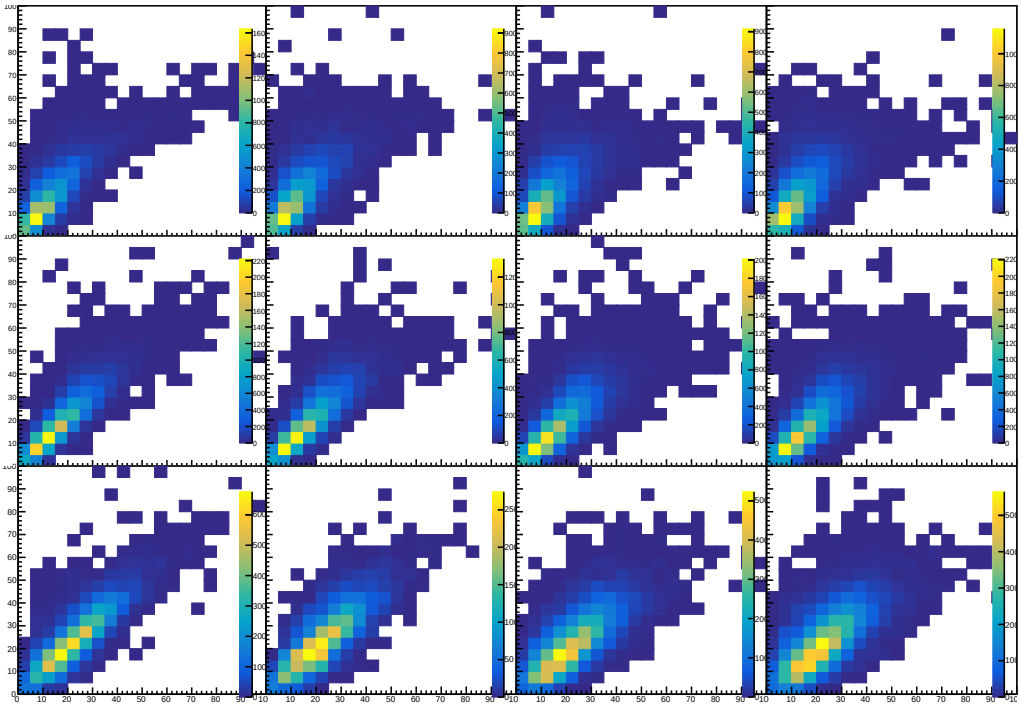

Figure 54: Migration matrix from TKU to TKD (recon).

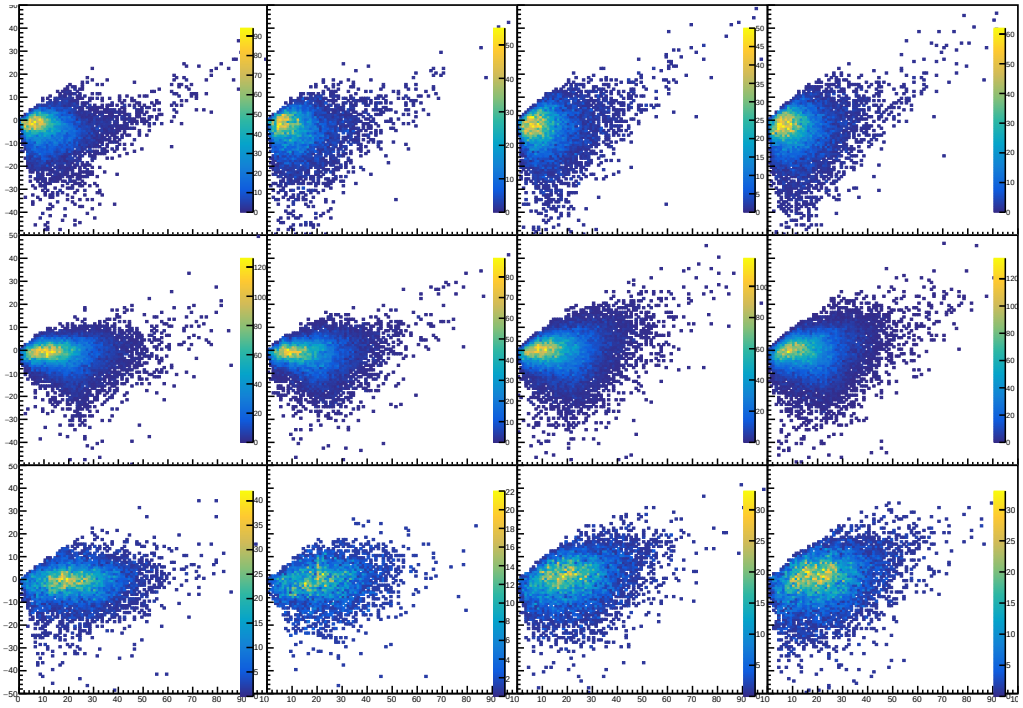

Figure 55: Change in amplitude (recon).

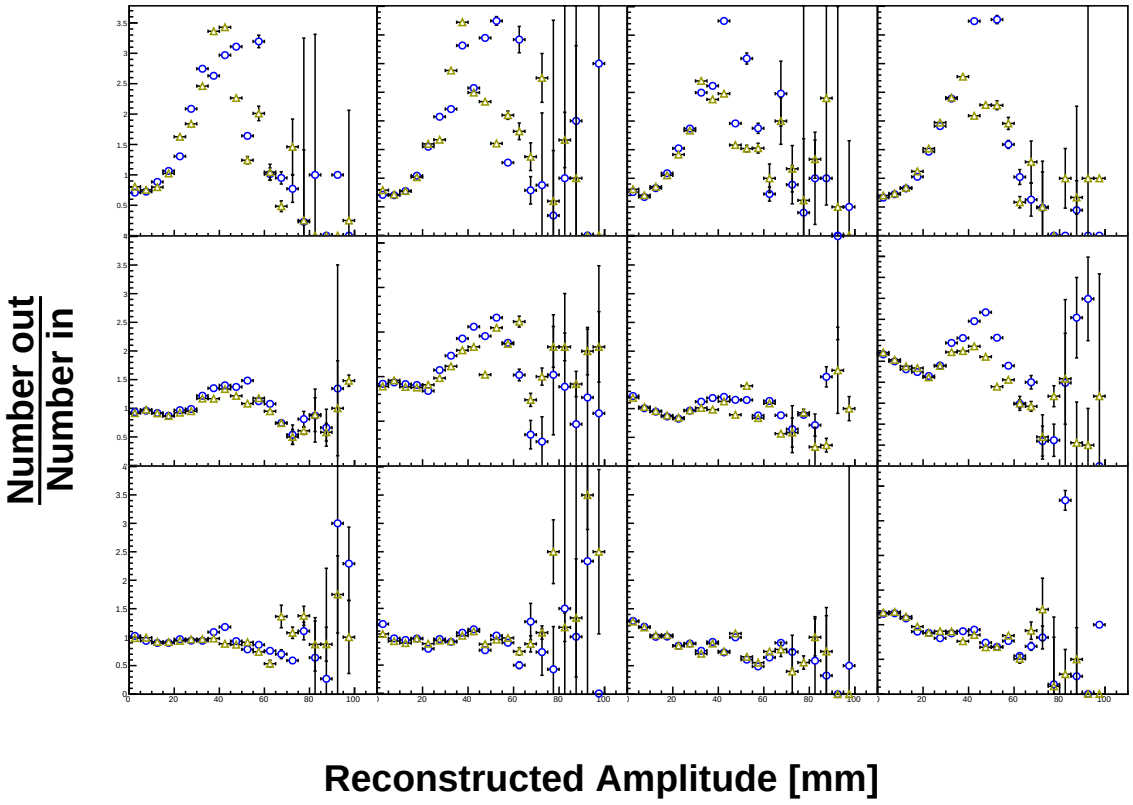

Figure 56: Ratio of amplitude PDFs; one line is data one is MC (recon).

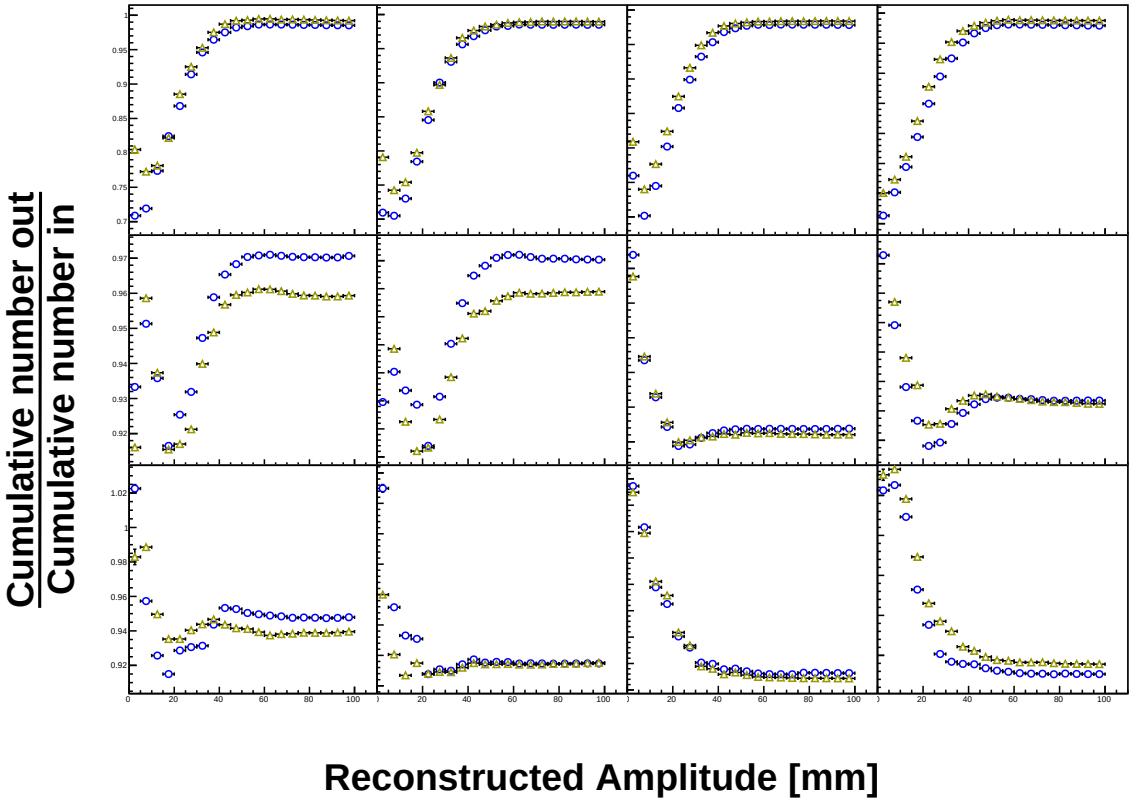

Figure 57: Ratio of amplitude CDFs; one line is data one is MC (recon).

We measure a given emittance change and try to tie it into a model. The model can be wrong because e.g. the fields were wrong, the absorber was wrong, etc. We have following sources of uncertainty:

- Field uncertainty (alignment, current, etc)
- Absorber uncertainty (thickness, density, etc)
- Other material budget
- Not sure, maybe if we are projecting upstream tracks we should include the uncertainty on the upstream measurement? This is a bit circular...

10 Conclusions

Author: Rogers

blah blah.

References

R. Roser, A. Name†
Fermilab, P.O. Box 500, Batavia, IL 60510-5011, USA
† *Also at another institute*

K. Long
Physics Department, Blackett Laboratory, Imperial College London, Exhibition Road, London, SW7 2AZ, UK